A STUDY OF THE THERMAL PROPERTIES OF COMMERCIALLY AVAILABLE MULTI-WALLED CARBON NANOTUBES AND GOLD NANOWIRES

By

Kyle Otte

Thesis

Submitted to the Faculty of the

Graduate School of Vanderbilt University

in partial fulfillment of the requirements

for the degree of

MASTER OF SCIENCE

in

Mechanical Engineering

August, 2013

Nashville, Tennessee

Approved:

Dr. Deyu Li

Dr. Greg Walker

Dr. Robert Pitz

TABLE OF CONTENTS

LIST OF TABLES

LIST OF FIGURES

Chapter 1

Literature Review

The study of one-dimensional (1-D) nanostructures is of fundamental scientific interest. Nanostructures, which include nanotubes, nanorods, nanowires, nanoribbons, and other geometries of different materials, could possess unique thermal, mechanical, and electrical properties when compared to their bulk counterparts. This is due to classical and quantum confinement effects. These unique properties of nanostructures could have profound impacts on energy conversion devices, as well as thermal management of microelectronic, optoelectronic, and photonic devices. Because of the vast potential that these novel materials hold, nanostructures have attracted a great amount of attention over the past two decades, particularly since the discovery of carbon nanotubes (CNTs) in 1991 (Iijima, 1991). Experimental measurements of the thermal properties of individual 1-D nanostructures pose significant challenges because of their extremely small size, which leads to difficulties in sample preparation, measurement, and classification.

This thesis seeks to shed some light on two difficult questions related to nanostructures. The first involves the state of industrially produced multi-walled carbon nanotubes (MWCNTs). While the research community still disagrees on what the maximum thermal conductivity of a perfect MWCNT would be, it is important to know the thermal properties of MWCNTs produced by commercial vendors, especially as more vendors enter the market and advertise high quality MWCNTs. The second issue involves the thermal contact resistance between two nanostructures. Metallic nanowires could

have high thermal conductivity, but when they form a point contact the thermal resistance at this point can be significant. This thesis seeks to analyze that thermal resistance. In the introduction section, we first briefly review the past research work that has been done in regards to thermal transport through 1-D carbon and metallic nanostructures.

1.1 Phonon Transport in Carbon Nanotubes

In determining the thermal properties of MWCNTs it is important to understand the underlying physical mechanism that allows thermal energy to be transported through a MWCNT. In MWCNTs, the dominant heat carrier is phonons, which are quantized lattice vibrations that play an important role in material heat capacity and thermal conductivity. Phonon transport in MWCNTs leads to thermal conduction, and thermal conductivity is determined by the total number of phonons available for transport, their velocities, and how much scattering phonons experience during their transport.

CNTs are expected to possess very high thermal conductivities due to their unique structures which almost eliminate the boundary scattering effect. Using molecular dynamics simulations with the Tersoff potential, Berber *et al.* (Berber, 2000) predicted that the thermal conductivity for a single (10, 10) nanotube could reach 6,600 W/m-K at 300 K. This is much higher than the thermal conductivity of diamond (2,200 W/m-K), which has the highest known thermal conductivity of any solid at room temperature. The prediction of the record high thermal conductivity of CNTs inspired efforts to experimentally measure the thermal conductivity of CNTs and the first experimental study of thermal transport through an individual MWCNT was conducted by Kim *et al* (Kim, 2001). They developed a suspended microfabricated device that utilized e-beam lithography to create two suspended heater and thermometer pads. Using probe

manipulation, a MWCNT was selected and measured. They demonstrated that a 14 nm-diameter MWCNT has a thermal conductivity of more than 3,000 W/m-K at 300 K, which is one order of magnitude greater than previous results from CNT mat samples.

Yu *et al.* (Yu, 2005) experimentally measured the thermal conductance of a ~1-2 nm-diameter single-walled CNT (SWCNT) with a suspended length of 2.76 μm. They compared their results to the calculated ballistic thermal conductance of a 1 nm-diameter SWCNT and found that the two results were very close. Signatures of phonon-phonon Umklapp scattering were not observed at temperatures between 110 K and 300 K. Pop *et al.* (Pop, 2006) extracted the thermal properties of an individual SWCNT and their results indicated a thermal conductivity of nearly 3,500 W/m-K at room temperature for a 2.6 μm suspended length sample with a diameter of 1.7 nm. They then heuristically calculated the length dependence of thermal conductivity as shown in **Figure 1.1**. They showed that at temperatures above the peak thermal conductivity, the thermal conductivity decreases at a rate close to 1/T.

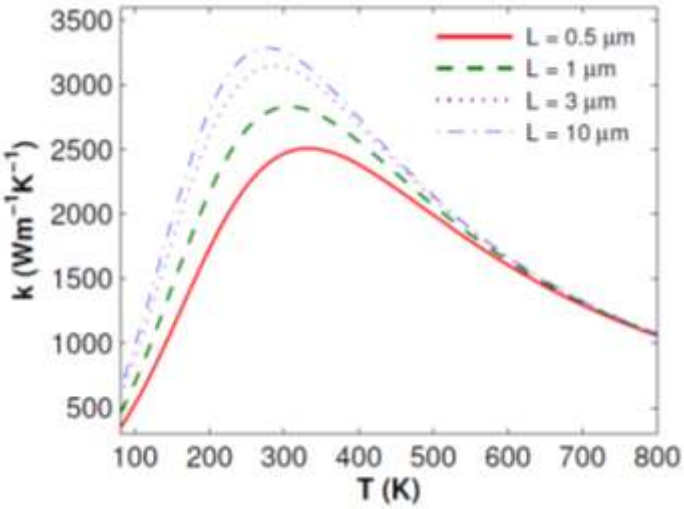

Figure 1.1 - Thermal conductivity of SWCNTs of different suspended lengths and 1.7 nm-diameter. (Pop, 2006).

Brown et al. (Brown, 2005) mechanically attached an arc-grown bundle of MWCNTs to a thermal probe. A temperature sensing scanning microscope probe was then used to obtain thermal measurements on individual MWCNTs by flowing energy down a MWCNT and recording the energy flow as a function of the temperature difference across it. This method demonstrates both ballistic phonon heat transport as well as electrical transport in MWCNTs.

Fujii *et al*. (Fujii 2005) measured the thermal conductivity of a single suspended CNT using a T-type nanosensor that is attached to the sample. The experimental results showed that the thermal conductivity of a CNT increases as its diameter decreases. The results also showed that the thermal conductivity can reach approximately 2,070 W/m-K for a CNT with a diameter of 9.8 nm. They also claimed that for a CNT having a diameter of 16.1 nm, the thermal conductivity approaches an asymptote at about 320 K, which was the highest temperature that they reached using their measurement setup. Chiu *et al.* (Chiu, 2005) determined that the thermal conductivity for a free-standing MWCNT to be approximately 600 W/m-K by fitting the measured electrical power to the inverse of the suspended length of the MWCNT. Three different lengths of MWCNTs ranging from 0.74 to 1.66 μm were measured and the tube diameters are approximately 10 nm. Choi *et al.* (Choi, 2006) used a four-point 3ω method to measure thermal properties of individual MWCNTs of 45 nm in diameter and 1 μm suspended length. The measured room temperature value of thermal conductivity was 300 ± 20 W/m-K.

Mingo *et al.* (Mingo, 2005) answered two important questions about thermal transport through CNTs. Fist, the ballistic lattice thermal conductance was quantized, and second the maximum length of a CNT for which phonon transport remains ballistic was

calculated. Both of these questions were answered by calculating the upper bounds of the lattice thermal conductance of SWCNTs, graphene, and graphite. These results showed that ballistic phonon transport in CNTs can be on the order of μm length below room temperature, and that the thermal conductance is much smaller than previously reported. The calculated theoretical ballistic conductance of graphite agreed well with the experimental results of MWCNTs below 200 K by a factor of 0.4, which suggests that MWCNTs and graphite have similar thermal conduction properties below 200 K. The thermal conductivity reduction of MWCNTs when compared with SWCNTs is most likely due to interactions between different layers and structural defects.

A hot wire probe for use inside a transmission electron microscope (TEM) that measures the thermal resistance of individual nanostructures was used by Dames *et al*. (Dames, 2007) to measure the thermal conductivity of a 30 nm-diameter MWCNT. The results yielded 17 W/m-K, which is significantly lower than other measurements. This small thermal conductivity was attributed to high contact thermal resistance at each end of the tube and the short length of the tube (0.38 μm).

It is worth noting that in many of the above-discussed measurements, the derived thermal conductivity is an effective one because an accurate estimation of the contact thermal resistance between the CNTs and the heat source/sink is not included. Therefore, the reported thermal conductivity tends to be lower than the intrinsic thermal conductivity of the CNTs.

One method that has been used to characterize MWCNTs and their quality is Raman spectroscopy. Raman spectroscopy is a spectroscopic technique used to observe rotational, vibrational, and other low-frequency modes in a system. It relies on inelastic

scattering, also called Raman scattering, of monochromatic light (usually 514 nm). The light interacts with the system and due to excitations in the system the energy of the laser photons is shifted up or down. Li *et al.* (Li, W. 1997) performed Raman characterization on aligned CNTs that were produced by chemical vapor deposition (CVD). They found that MWCNTs have a strong sharp peak at about 1,581 cm^{-1} which is called the G-peak. The MWCNTs also exhibited strong peaks at 2,687 cm^{-1} (G′ peak) and 1,348 cm^{-1} (D peak). The origin of the G′ and D peaks are explained as disorder-induced features due to the finite particle size effect or lattice distortion. In other words, the relative intensity of the D peak to the G peak is related to the crystal planar domain. If this ratio is low then the MWCNT is composed of well-aligned cylindrical tubes. If this ratio is high then there are many defects present and thus the thermal conductivity will most likely be low.

This section of literature review is relevant to the work presented in this thesis because this thesis seeks to report on the quality (from a heat transfer point of view) of MWCNTs currently produced by commercial vendors. Therefore we seek to compare the experimentally and numerically derived values of thermal conductivity in literature to that of real samples that can be readily purchased at large volume at this time. One tool that is used in this thesis to help characterize MWCNT quality is Raman spectroscopy.

1.2 Thermal Transport in Metallic Nanostructures

Even though metal nanowires do not receive as much attention as semiconducting nanomaterials or CNTs, they are important components in nanorobotics and nanocircuits. While the dominant energy carriers in semiconducting materials and CNTs are phonons, metals are fundamentally different. In pure metals electrons carry more of the heat

current than phonons at every temperature (Kittel, 2005). The thermal conductivity of a metal is derived as

$$\kappa_{el} = \frac{\pi^2}{3} \frac{n k_B^2 T \tau}{m} \qquad 1.1$$

where n is the electron concentration, k_B is Boltzmann's constant, T is temperature, τ is the collision time, and m is the mass of an electron.

Stewart and Norris (Stewart, 2000) studied the influence of radius on the thermal conductivity of thin metallic wires. They solved the Boltzmann transport equation for electrons and found that for metals commonly used in microelectronics such as Al, Ag, and Au, the thermal conductivity is reduced in wires with diameters of roughly 0.5 μm or less. They claim that when the diameter of the thin wire is on the same order of the electron mean free path, the thermal conductivity drops by roughly half of the bulk thermal conductivity. This work was done in simulations only and not in conjunction with experiments.

Lu *et al*. (Lu, 2002) concluded that the thermal conductivity of a gold nanowire is directly proportional to its size. An expression is presented for the reduction in conductivity due to the increase in boundary scattering. **Figure 1.2** shows the results that are obtained from this work.

In the figure, the value of ε represents the probability that the carrier is undergoing a specular scattering event at the interface and thus ranges from 0 to 1. D is the proportionality constant defined as the side length of a square wire divided by the average in-plane grain diameter. R is the reflection coefficient of the conduction electrons, which strike the grain boundaries. Therefore R can have values between 0 and

1. The size of nanowires studied in this experiment range from 15-80 nm x 20 nm x 500 nm.

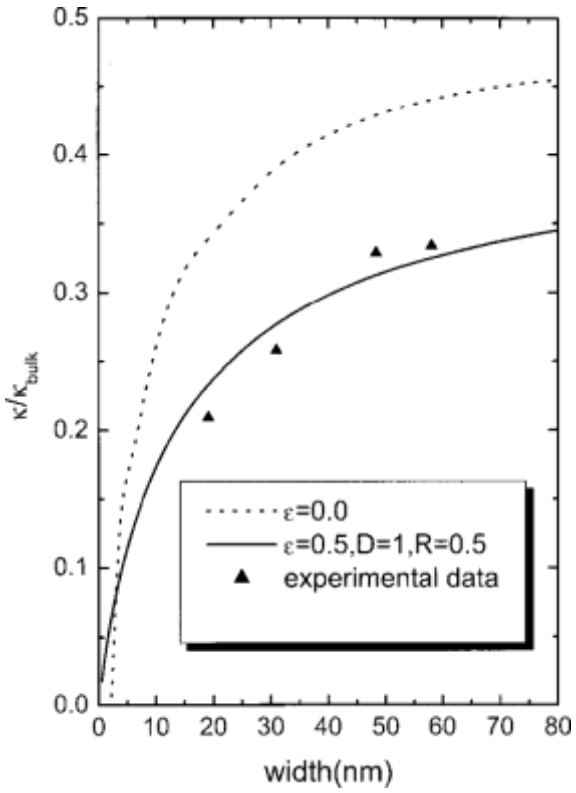

Figure 1.2 - The thermal conductivity ratio of gold nanowires to the bulk material for diffusive scattering surface with grain boundaries (Lu, 2002).

Bulk metal thermal conductivity follows the Wiedemann-Franz law which states that the ratio of the electronic contribution of the thermal conductivity (κ) to the electrical conductivity (σ) of a metal is proportional to temperature (T) as:

$$\frac{\kappa}{\sigma} = LT \qquad 1.2$$

where L is the Lorenz number and is equal to 2.44 x 10^{-8} W Ω K^{-2} at temperatures above the Debye Temperature.

Zhang *et al.* (Zhang, 2006) measured the electrical and thermal conductivities of polycrystalline gold nanofilms by a direct current heating method. They found that both the electrical and thermal conductivities are greatly reduced from the corresponding bulk values. This reduction becomes more evident at lower temperatures because the electron mean free path increases with decreasing temperature. Therefore the size effects become strengthened as the nanofilm thickness is comparable to the electron mean free path at 37 nm. Both surface and grain boundary scatterings are credited with the reduction in conductivities.

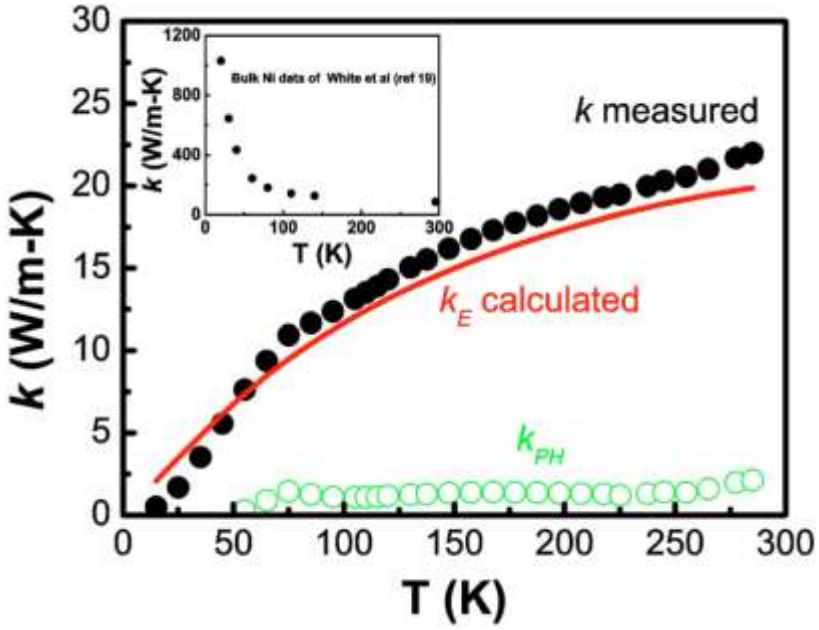

Figure 1.3 - Thermal Conductivity of nickel nanowire showing both electronic contributions as well as contributions from phonons (Ou, 2008).

Ou *et al.* (Ou, 2008) measured the thermal and electrical resistivity of nickel nanowires that were 100 nm x 180 nm and 35 μm long. Once again the thermal conductivity is significantly reduced from the bulk value. The reduction goes from approximately one order of magnitude at 300 K to more than two orders of magnitude at

around 30 K. The Lorenz number for such small nanowires is slightly higher than the normal Lorenz number of 2.44 x 10^{-8} W Ω K^{-2}. The Lorenz number of the nanowires stayed constant from 75 K to 300 K. Below 75 K the mean free path of the electrons becomes comparable to the grain size of the metal and the scattering is increased.

Figure 1.3 shows a plot of the thermal conductivity of a nickel nanowire vs. temperature. The electronic contribution to the thermal conductivity is calculated using the Wiedemann-Franz law and then the contribution to thermal conductivity from phonons is calculated by subtracting the electronic contribution from the total thermal conductivity. The higher value for the thermal conductivity due to electrons at low temperatures indicates a violation of the Wiedemann-Franz law at these temperatures. At all temperatures the contribution to heat conduction from phonons is less than 10% of the total.

This thesis seeks to compare the thermal conductivity of gold nanowires to that reported in the literature. It also seeks to analyze the thermal resistance of a point contact in crossed gold nanowires. This work will deepen our understanding of nanoscale heat transport through metallic nanowires.

1.3 Contact thermal resistance

In 1936, Kurti *et al.* (Kurti, 1936) expressed the idea that a thermal resistance might exist at the interface between liquid helium and a solid. They stated that the resistance was very small and therefore did not study it any further. Shortly thereafter Keesom *et al*. (Keesom 1936) stated that the thermal resistance at this boundary was "relatively very considerable", but they also did not pay further attention to the

phenomenon to obtain a deeper understanding. Finally, in 1941 Kapitza reported measurements that he conducted related to a temperature drop near the boundary between helium and a solid as heat crossed this boundary. Today this resistance is called the Kapitza resistance (Swartz, 1989). The idea for boundary thermal resistance is quite simple. In the presence of a heat flux J (W/m^2) across a boundary, the boundary thermal resistance creates a temperature discontinuity ΔT at the boundary. The thermal boundary resistance (TBR) is defined as $R_B = \Delta T/J$.

The idea of TBR is quite intuitive. An interface represents a departure from the regular crystalline lattice through which heat carriers propagate. For an interface between dissimilar materials, the different densities, lattice constants, and therefore sound speeds result in a mismatch in acoustic impedances, similar to the mismatch in the refractive indices of two optically different materials.

Two commonly used models have been developed to model the boundary scattering of phonons, and therefore the TBR. First, the diffuse mismatch model states that when phonons strike a boundary they lose all "memory" of where they come from. Therefore the probability of phonons being scattered to one side of the boundary or the other is simply proportional to the phonon density of states of each material. In contrast, the acoustic mismatch model (AMM) states that no scattering takes place at the interface. The appropriate stress and boundary conditions are applied at the interface to solve for a transmission coefficient, t_{AB}, for phonon energy in material A incident normal to the interface with material B. In the AMM, the interface simply connects two different materials, and all thermal resistance stems from the differences between these two

materials. In the AMM, the fraction of energy transmitted is independent of the structure of the interface itself (Cahill, 2003).

With the development of microelectronic industry, thermal management of microelectronic devices poses significant challenges. With the aggressive miniaturization, there are many interfaces in these devices and interface thermal resistance has attracted tremendous attention in the past two decades. Many experimental studies have been carried out to understand the effects of different parameters on the interface thermal resistance.

For example, Swartz et al. (Swartz, 1987) measured the solid-solid thermal boundary resistance between Rh:Fe and polished sapphire spanning a temperature range from 1 to 300 K. Below 30 K the TBR was found to be in agreement with the prediction of the AMM. Above 30 K the TBR was found to decrease less rapidly with increasing temperature than predicted by theory. Ravi Prasher (Prasher, 2008) used the properties of graphite to calculate the thermal boundary resistance between a MWCNT and the measuring device and achieved results in very good agreement with the experimental data of Kim *et al*. (Kim, 2001). The intrinsic mean free path of phonons in MWCNTs in the temperature range of 10 to 100 K was found to be similar to that of graphite.

Recently contact thermal resistance between individual nanostructures attracted much attention because of its important role in thermal properties of nanocomposite materials. In fact, the early thermal measurements on CNTs were performed on mats or ropes of CNTs and thus a "bulk" thermal conductivity was derived, which is much smaller than the intrinsic thermal conductivity of an individual MWCNT because of the thermal resistance associated with numerous contacts. On this front Yang *et al.* (Yang,

2010) have conducted experiments to derive the contact thermal resistance between two individual MWCNTs.

The authors measured the contact thermal resistance between two individual MWCNTs forming different contact morphologies. The first was a crossed contact with a calculated contact area of 118 nm^2, and the second was an aligned contact with a calculated contact area of 2.96×10^4 nm^2.

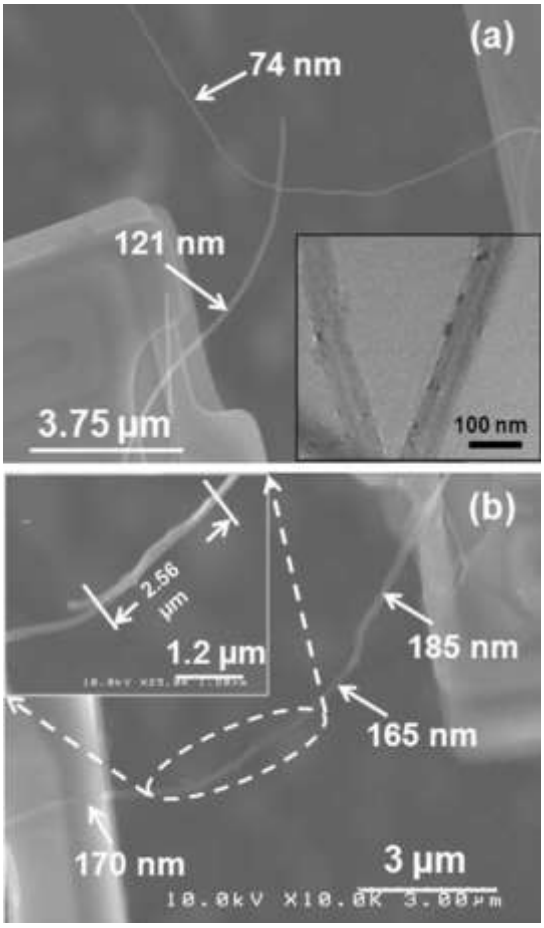

Figure 1.4 - SEM micrographs of two individual CNTs forming a contact between two suspended membranes. a) a cross contact, and b) an aligned contact with a 2.56 µm overlap. The inset in a) is a TEM image of some sample batch CNTs (Yang, 2010).

Figure 1.4 shows an SEM micrograph of the two different configurations of nanotubes. The thermal conductivities of individual MWCNTs from the same batch samples were measured separately with a single tube aligned across the two suspended membranes.

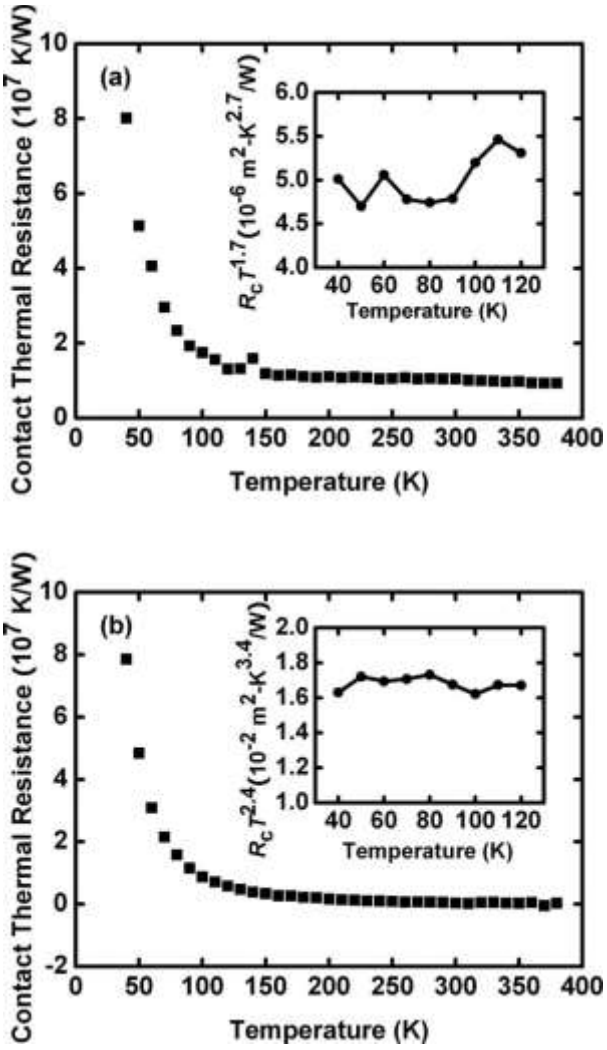

Figure 1.5 - The measured total contact thermal resistance as a function of temperature of a) the cross contact; and b) the aligned contact. The insets show the dependence of the contact thermal resistance per unit area. (Yang, 2010).

Figure 1.5 shows the contact thermal resistance as a function of temperature for the two samples measured. As the temperature drops towards about 120 K, the contact thermal resistance increases slightly and then as temperature further drops below 120 K it increases very rapidly.

The work presented in this thesis involves the contact resistance between gold nanowires. Therefore, it is important to understand the previous work done in this area. The method developed by Yang *et al.* (Yang, 2010) of determining the contact thermal resistance between two nanostructures is utilized in this thesis.

1.4 Summary

In the past decade, studies of thermal transport in 1-D nanostructures have led to an increase in understanding of nanoscale thermal transport phenomena. However, contact thermal resistance remains an important and difficult problem in determining the intrinsic thermal conductivity of individual nanostructures as well as the heat transport characteristics of nanostructure-containing mixtures and composite materials. Also, the wide range of reported thermal conductivity values of MWCNTs begs the question: what is the current state of the industrial production of MWCNTs?

In order to begin to address these important issues we conduct an extensive study of the MWCNTs currently available from a plethora of resources. We also try to extract the thermal resistance of a point contact between two gold nanowires to gain a better understanding of the impact of nanoscale constrictions on electron dominated heat transport.

Chapter 2

Measurement Setup

In order to measure the thermal conductivity of bulk materials, most measurement techniques involve creating a temperature gradient within the sample that is measured by strategically placed thermocouples. Bulk samples can also be characterized by comparing the temperature gradient within a sample to the temperature gradient of a sample with a known thermal conductivity. In order to measure the thermal conductivity of thin films, several techniques have been developed (Mirmira, 1998). A temperature gradient can be created within the film by either laser heating or Joule heating with electric current flowing through a thin metal line. The induced temperature gradient can then be measured by either resistance thermometers or the change in the film's reflectivity. While these techniques work well for bulk samples or thin films, they are not practical for measuring the thermal conductivity of one dimensional (1-D) nanostructures due to the small size of such nanostructures. Shi *et al.* (Shi, 2003) developed a suspended microdevice that can be used to measure the thermal conductivity and thermoelectric properties of individual 1-D nanostructures. The technique is essentially a thermal bridge method in which the sample serves as a component in a thermal resistance network and the thermal conductivity of the sample can be extracted from the derived thermal resistance of the sample. This chapter outlines the design and working mechanism of this device as well as the measurement technique utilized to obtain the results presented in this thesis.

2.1 Device Design

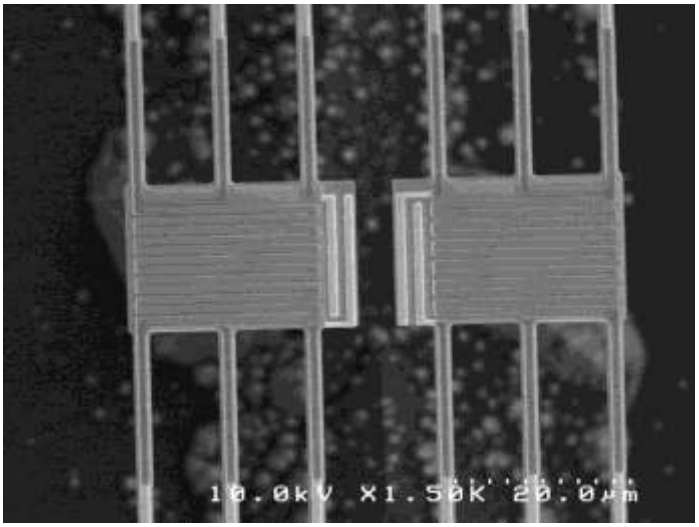

Figure 2.1- An SEM micrograph of the suspended microdevice with integrated resistance heaters and thermometers.

Figure 2.1 shows a Scanning Electron Microscopy (SEM) image of the microdevice that can be used for measuring electrical as well as thermal conductivities and Seebeck coefficients. Each device consists of two adjacent 18.2 µm x 27.1 µm low stress silicon nitride (SiN_x) membranes which are suspended using six 0.5 µm thick, 416 µm long and 2.2 µm wide SiN_x beams. Each membrane holds one platinum resistance thermometer (PRT) that is composed of 30 nm thick and 500 nm wide platinum lines arranged in a serpentine pattern. In order to prevent electrically conductive samples such as multi-wall carbon nanotubes (MWCNTs) or gold nanowires from shorting the heater coils and disturbing the measurement circuits, the PRT area is covered by a 200 nm thick low temperature silicon oxide (LTO) layer. The PRT is connected via 1.2 µm wide platinum leads on each SiN_x beam to 400 µm x 500 µm platinum contact pads that are located on the substrate.

2.2 Sample Preparation

In order to measure the thermal properties of nanostructures using the above device, a 1-D nanostructure must be placed on the device so that the nanostructure spans the two suspended membranes. This is often the most difficult step in the measurement process, especially when attempting to arrange nanostructures in a crossed configuration with a point contact. The process requires a deft touch and a significant amount of practice and patience to become proficient at the manipulations.

The sample placement process is composed of two main steps. First, a very small amount of 1-D nanostructures are suspended in a solution such as reagent alcohol or isoproponal alcohol (IPA). Distilled water can also be used depending on the sample, although it requires more time for evaporation. This mixture is then sonicated using a Cole Parmer 8891 ultrasonic cleaner for a short amount of time in order to better disperse the 1-D nanostructures and form a uniform suspension. Most nanostructures cannot be sonicated for long periods of time because the input of sonic energy into the sample will break the nanostructures into small pieces. Several drops of this solution are then casted onto a small piece of polydimethylsiloxane (PDMS). After the alcohol has evaporated, many 1-D nanostructures are laying on the edges of the PDMS. Because cured PDMS is transparent, we can use this PDMS block with nanostructures resting on it to locate single, undamaged nanostructures for measurement.

The second step in the sample preparation process is to use a sharp tip with a radius of ~0.1 μm to pick up single nanostructures and transfer them to the microdevice for thermal transport measurement. The van der Waals interactions between the tip and the nanostructures allow them to be picked up and transported.

Figure 2.2– An in-house built manipulator in conjunction with a Nikon microscope used to manipulate nanostructures.

Figure 2.2 shows an in-house built micromanipulator which can be used to move nanostructures from a substrate to a measurement device. The device has very fine adjustment screws in three dimensions that can be used to guide the tip to exact locations and pick up a nanostructure via van der Waals force without damaging it. Another advantage of casting the nanostructures onto PDMS is that PDMS is a rubber-like substance which will deflect under pressure from the manipulator tip, meaning that the tip is not damaged every time a nanostructure is picked up.

Figure 2.3 shows a MWCNT sample placed between the two suspended membranes using the micromanipulator. The whole process is performed under a 100x, long working distance (6.5 mm) objective lens that is mounted on a Nikon optical microscope.

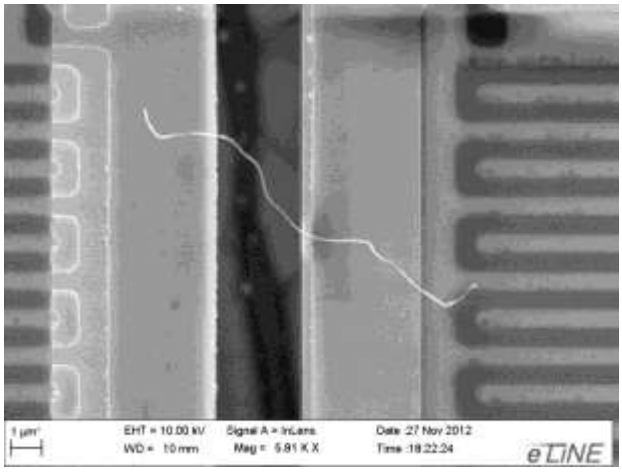

Figure 2.3- A MWCNT sample placed between the two suspended membranes.

2.3 Measurement Setup

Figure 2.4 shows the schematic diagram of the measurement setup. The microdevice with a 1-D nanostructure between the two suspended membranes serving as a heating and a sensing membrane, respectively is glued onto a dual in-line package (DIP) and 1% Si/Al wire is used to electrically connect the microdevice to the DIP. The entire DIP is then placed in a cryostat and the chamber pressure is pumped down to a pressure below 10^{-6} Torr. The voltage change on the platinum resistance thermometers is measured using two Stanford Research SR850 lock-in amplifiers. One amplifier is connected to the heating side membrane and one is connected to the sensing side membrane. A DC heating current is coupled with a small sinusoidal AC signal from the heating side lock-in amplifier through an integrated differential amplifier (Analog Devices SSM2141). This voltage is then passed through a 500 kΩ resistor on the heating side and a 1 MΩ resistor on the sensing side. These large resistors enable us to assume a constant current condition for each DC heating voltage.

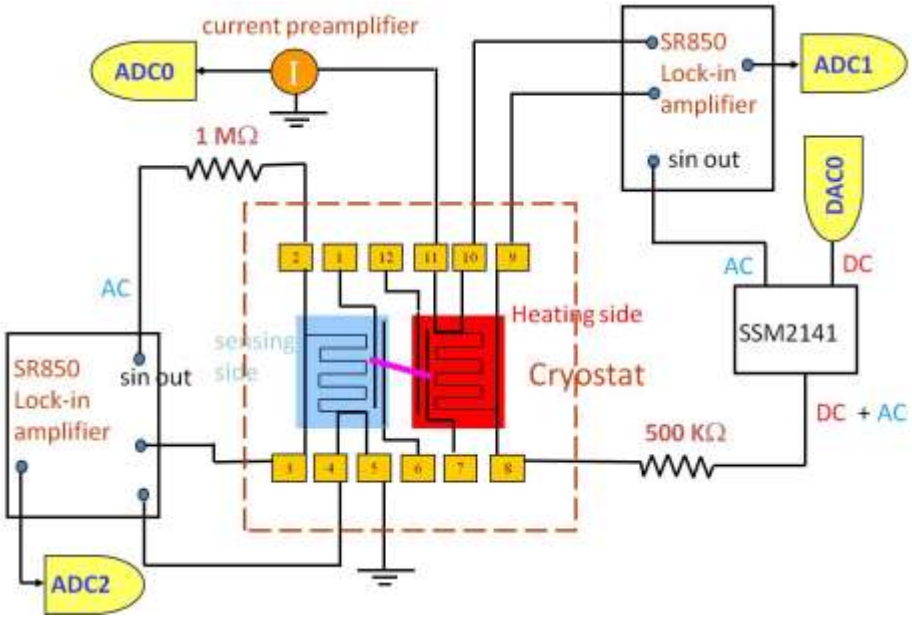

Figure 2.4- Schematic of the measurement setup.

The thermal circuit of the measurement setup is shown in **Figure 2.5**. A DC current (I) passes through the left membrane serving as the heating side, which leads to Joule heating ($Q_h = I^2R_h$, where R_h is the PRT's electrical resistance) in the PRT on the heating side. This heat is dissipated by conduction along the six supporting beams as well as some heat conduction through the sample to the sensing side membrane on the right side. If the measurement is performed at a high vacuum and the change in temperature of the heating side is small ΔT_h ($\Delta T_h = T_h - T_0 < 5$ K), radiation as well as conduction/convection through the residue air are negligible (Shi, 2003).

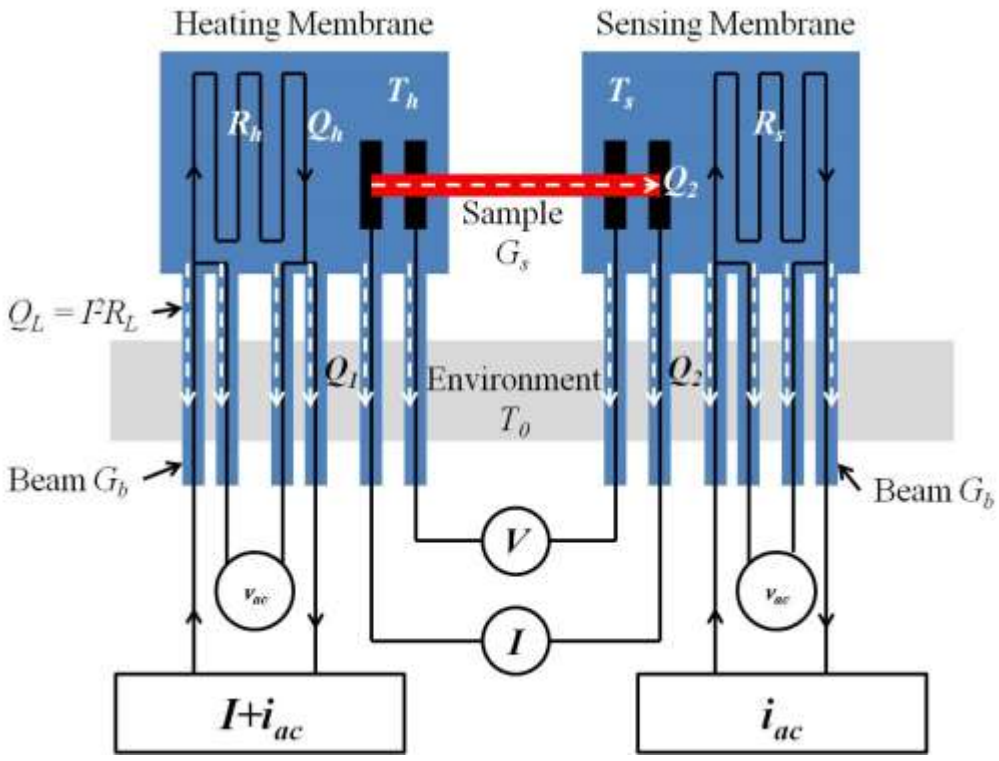

Figure 2.5- Thermal circuit for the measurement setup.

Each membrane is connected to the contact pads by four 1.2 μm wide Pt leads, which allows for a four probe resistance measurement. The two leads through which the DC current flows are also heated by Joule heating in the amount of $2Q_L = 2I^2R_L$. R_L is the resistance of each of the Pt leads, which is about half of R_h. Since the thermal resistance of the long SiN_x beams is much higher than the internal thermal resistance of the heating and sensing membranes, using the lump capacitance method we can say that the temperature of the heating membrane is raised to some uniform temperature T_h. As heat Q_2 is conducted through the sample the temperature of the sensing membrane is raised to some uniform temperature T_s. The heat transferred to the sensing membrane is further conducted through the six beams that support the sensing membrane to the substrate. The

remaining heat, i.e. $Q_1 = Q_h + 2Q_L - Q_2$, is conducted to the environment through the other six beams that suspend the heating membrane. The total Joule heat is therefore

$$Q_{tot} = Q_h + Q_L = I^2(R_h + 2R_L) \qquad 2.1$$

The six beams that support each membrane are identical. The total thermal conductance of the six beams can then be written as $G_b = R_b^{-1} = 6k_lA/L$, where k_l, A, and L are the thermal conductivity, cross sectional area, and length of each beam, respectively.

Using the thermal circuit shown in **Figure 2.5** the heat conducted through the nanostructure can be written as

$$Q_2 = G_b (T_s - T_0) = G_s (T_h - T_s) \qquad 2.2$$

where G_s is the total thermal conductance of the sample, which is what we want to measure. This conductance includes both the intrinsic thermal conductance as well as the contact thermal resistance between the nanostructure and the two suspended membranes. Therefore G_s can be written as

$$G_s = \frac{1}{R} = \left(\frac{1}{G_n} + \frac{1}{G_c}\right)^{-1} \qquad 2.3$$

where $G_n = k_nA_n/L_n$ is the intrinsic thermal conductance of the nanostructure, k_n is the thermal conductivity, A_n is the cross sectional area, and L_n is the length of the sample that is suspended between the two membranes. G_c is the contact thermal conductance between the 1-D nanostructure and the two suspended membranes. Because the temperature rise ΔT_h is small at each measurement temperature point, G_s, G_b and G_c are assumed to be constant as ΔT_h is ramped up.

Likewise, from the heating membrane we have

$$Q_1 = G_b (T_h - T_0) \qquad 2.4$$

Adding Eq. 2.2 and 2.4 yields

$$Q_{tot} = Q_1 + Q_2 = G_b(\Delta T_h + \Delta T_s) \qquad 2.5$$

where $\Delta T_s \equiv T_s - T_0$ and

$$G_b = \frac{Q_{tot}}{\Delta T_s + \Delta T_h} = \frac{Q_h + Q_L}{\Delta T_s + \Delta T_h} \qquad 2.5$$

Therefore

$$G_s = \frac{\Delta T_s}{\Delta T_h - \Delta T_s} G_b \qquad 2.6$$

Q_h and Q_L can be calculated readily from the measured current and voltage drops across the heating PRT and the PT leads. ΔT_h and ΔT_s are calculated from the measured resistances of the two PRTs and their temperature coefficient of resistance *(TCR≡dR/dT)/R)*. The four-probe electrical resistance R_s of the sensing PRT is measured using one of the SR850 lock-in amplifiers with a ~300 nA 637 Hz sinusoidal excitation current. The rise in temperature of the sensing membrane ΔT_s is a function of the DC current (I) of the heating PRT, and is related to R_s according to the equation

$$\Delta T_s = \frac{\Delta R_s(I)}{R_s(I) \times TCR}; \quad \Delta R_s(I) \equiv R_s(I) - \Delta R_s(0) \qquad 2.7$$

Similarly, the temperature rise ΔT_h of the heating membrane can be calculated by

$$\Delta T_h = \frac{\Delta R_h(I)}{R_h(I) \times TCR}; \quad \Delta R_h(I) \equiv R_h(I) - \Delta R_h(0) \qquad 2.8$$

A 300-500 nA sinusoidal current, i_{ac}, with a frequency f can be coupled to the much larger DC heating current. One of the SR850 lock-in amplifiers is used to measure the first harmonic component (v_{ac}) of the voltage drop across the heating PRT, yielding $R_h = v_{ac}/ i_{ac}$. In order to obtain R_h from this method, it can be shown that

$$\Delta T_h(I) = \frac{\Delta R_h(I)}{3\frac{dR_h}{dT}}, \text{ for } f << \frac{1}{2\pi\tau} \qquad 2.9$$

and

$$\Delta T_h(I) = \frac{\Delta R_h(I)}{\frac{dR_h}{dT}}, \text{ for } f >> \frac{1}{2\pi\tau} \qquad 2.10$$

where τ is the thermal time constant of the suspended device, and is estimated to be on the order of 10 ms. The first harmonic modulated heating component, i.e. $2i_{ac}IR_h$ causes the difference between these two solutions for different frequency ranges. At a very low frequency compared to $1/(2\pi\tau)$, the modulated heating yields a nontrivial first harmonic component in T_h. This further causes a nontrivial first harmonic oscillation in R_h. At a very high frequency compared to $1/(2\pi\tau)$, the modulated heating yields a trivial first harmonic component in T_h. This effect gives rise to a factor of 3 differences in ΔR_h measured by the lock-in method. In addition, τ is proportional to C/k, and k is proportional to Cl. C is the heat capacity, k is thermal conductivity, and l is the phonon mean free path which increases with decreasing temperature. Hence, τ is proportional to $1/l$ and decreases with decreasing temperature. Therefore, the transition between the two solutions in Eqs. 2.9 and 2.10 occurs at an increased frequency as the temperature decreases. In practice, we use f = 1400 Hz, for which Eq. 2.10 is valid in the temperature range of 20 - 420 K. Since all results presented in this thesis are obtained between 150 K and 320 K, this value of f is valid.

2.4 Measurements of Intrinsic Thermal Conductivity

Using the method outlined by Yang *et al.* (Yang, 2011) the intrinsic thermal conductivity of an individual nanostructure and its contact thermal resistance with the heat source/sink can be extracted with multiple measurements of the same sample with

different suspended lengths between the heat source and heat sink. Assuming that the contact thermal resistance does not change with different measurements the total resistance can be written as

$$R_{tot} = R_{CM} + R_{CNT/L} \times L_M \qquad 2.11$$

where R_{tot} is the total measured thermal resistance including the intrinsic thermal resistance of the nanostructure segment as well as the contact thermal resistance with the two membranes. R_{CM} is the sum of the contact thermal resistances with the two membranes. $R_{CNT/L}$ is the intrinsic thermal resistance of the nanostructure per unit length, and L_M is the suspended length of the sample between the two membranes.

After two measurements with two different suspended lengths we can calculate $R_{CNT/L}$ as

$$R_{CNT/L} = (R_{tot1} - R_{tot2}) \,/\, (L_{M2} - L_{M1}) \qquad 2.12$$

and

$$R_{CM} = (L_{M2}R_{tot1} - L_{M1}R_{tot2}) / \,(L_{M2} - L_{M1}) \qquad 2.13$$

where R_{tot1} and R_{tot2} are the measured total thermal resistances from the two different measurements, and L_{M1} and L_{M2} are the corresponding nanostructure lengths between the two membranes in each measurement.

Finally, using the fin heat transfer model, R_{CM} can be written as

$$R_{CM} = \frac{2\sqrt{R_{CNT/L} \cdot R_C'}}{\tanh\left(L_C \sqrt{\frac{R_{CNT/L}}{R_C'}}\right)} \qquad 2.14$$

where L_c is the length of the nanostructure segment in contact with the membrane and R_c' is the contact thermal resistance per unit length. When L_c is large enough so that the

denominator in Eq 2.14 can be approximated as unity, R_c' is no longer a function of the contact length. The function *tanh (x)* is very close to unity for $x = 2$ and approaches unity slowly in an asymptotic manner for $x \geq 2$. Therefore, the minimum contact length $L_{c,min}$ can be estimated as

$$L_{c,min} = 2/\sqrt{R_{CNT/L}/R_c'} \qquad 2.15$$

In this thesis, this methodology of extracting intrinsic thermal conductivities was utilized for both MWCNTs as well as gold nanowires. From an experimental standpoint the most difficult part of this method was the successful manipulation of a sample to get different suspended lengths between the heating and sensing membranes.

Chapter 3

Thermal Conductivity of Multi-Walled Carbon Nanotubes

Carbon nanotubes (CNTs) have been intensively studied for the past two decades due to their excellent thermal, mechanical, and electrical properties. One of the effects of this concentrated research has been the proliferation of startup companies producing CNTs in order to make a profit. A quick Google search can turn up over a dozen companies eager to sell CNTs of all varieties. This large amount of commercially available CNTs begs the question: Are these tubes of high quality? While researchers still debate the exact values of thermal properties of an ideal CNT, it is commonly believed that high-quality CNTs should have high thermal conductivity. However, it is not clear about the quality of the CNTs for sale on the market today and a study of the thermal conductivity of these CNTs is important for their applications related to thermal transport such as for thermal interface materials (TIM) and CNT-based composites targeting high thermal conductivities.

For example, a group of NASA researchers are working on a project using multi-walled CNTs (MWCNTs) to enhance the thermal conductivity of NARloy-Z (Cu-3%Ag-0.5%Zr alloy), which is the state of the art material used to make the liner of the liquid rocket engine combustion chamber. Based on the results of the NASA group, the CNT-NARloy-Z composites have a lower, instead of higher, thermal conductivity than NARloy-Z itself. It is intriguing to see this unexpected observation and we suspect that one possible reason is that the MWCNTs used are of low quality and do not have a high thermal conductivity as expected.

In response to the need of understanding the thermal conductivity of MWCNTs that are available on the market, we have studied a total of 14 MWCNT samples from different sources. Two samples (General Nano and Pyrograf) were donated through the NASA group, and the sample from Pyrograf was used in CNT-NARloy-Z composites. Another sample was donated from a lab at Case Western University, while others were either donated by or purchased from the companies. **Table 3.1** gives general information about each sample received.

Table 3.1- MWCNT vendors and general specifications

Vendor	Claimed Diameter	Claimed Length	Raman	Measurement	TEM
Cheaptubes	50-80 nm	10-20 μm	Yes	No	No
Cheaptubes Graphitized	50-80 nm	10-20 μm	Yes	Yes	Yes
US Research Nanomaterials Inc.	30-50 nm	10-20 μm	Yes	No	No
Nanostrucutred & Amorphous Matls.	50-80 nm	10-20 μm	Yes	Yes	No
SES Research	40-60 nm	1-20 μm	Yes	No	No
HELIX Material Solutions	60-100 nm	0.4-40 μm	Yes	No	No
IoLiTec	40-60 nm	5-15 μm	Yes	No	No
NanoCS	40-60 nm	10-20 μm	Yes	No	No
MKNano	>50 nm	10-30 μm	Yes	No	No
Sigma-Aldrich	110-170 nm	5-9 μm	Yes	Yes	Yes
Nanoshel	4-12 nm	5-15 μm	Yes	Yes	Yes
Nanoshel Arc-Discharged	60-100 nm	5-15 μm	Yes	Yes	Yes
Ted Pella	4-12 nm	5-15 μm	Yes	No	No
General Nano	N/A	N/A	Yes	No	Yes
Pyrograf	N/A	N/A	Yes	Yes	Yes
Case Western University	N/A	N/A	Yes	Yes	Yes

Each sample was first characterized using Raman spectroscopy. A small portion of the sample was subjected to Raman spectroscopy studies and data were collected from five different spots. Two examples of the Raman results are presented in **Figure 3.1** (The complete results of the Raman spectroscopy for all samples are included in **Appendix A**.) The most relevant parameter from the Raman analysis of the CNT quality is the D/G ratio. From **Figure 3.1**, it can be seen that the first prominent peak is the D peak, which stands for dislocation or disorder, while the G peak represents the sp^2 bonds between carbon atoms in graphitic layers. If the D/G ratio is small that usually means that the MWCNTs are of high quality with few defects. If the ratio is large then the MWCNTs are most likely of low quality and will have a low thermal conductivity.

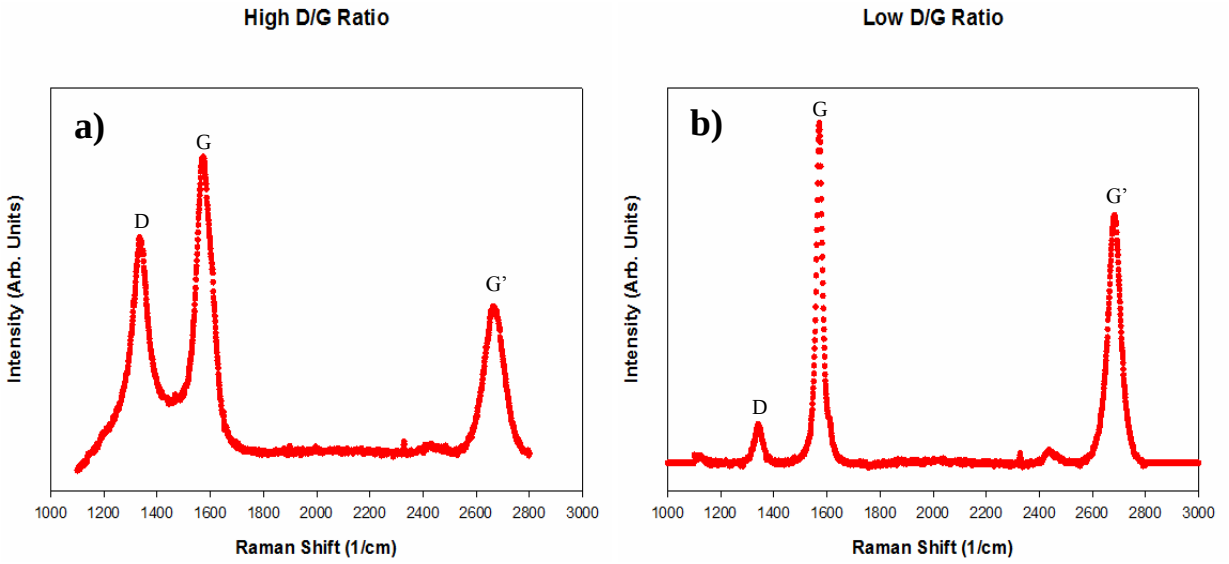

Figure 3.1- Samples of Raman spectrograph for samples with a) the highest D/G ratio (General Nano), as well as b) the lowest D/G ratio (Cheaptubes Graphitized).

Figure 3.1a presents the Raman results from spot 1 of the General Nano sample. The average D/G ratio over 5 spots from the General Nano sample is 1.010, which is the

highest among the MWCNTs we have obtained. This sample is also not cylindrical and appears to have poor structure. **Figure 3.1b** presents the Raman results from spot 1 of the Cheaptubes Graphitized sample. The average D/G ratio from the Cheaptubes Graphitized sample is 0.128, which is among the lowest ratio among all the samples we have obtained. This sample has a thermal conductivity that ranks among the highest from the samples that we have measured. **Table 3.2** gives the ratio of D peak to G peak at each spot from the Raman Analysis for all obtained MWCNT samples and the average based on these five spots.

Table 3.2- Raman analysis data for each vendor

Vendor	Spot 1	Spot 2	Spot 3	Spot 4	Spot 5	Average
Cheaptubes	0.551	0.604	0.597	0.614	0.604	0.594
Cheaptubes Graphitized	0.114	0.118	0.164	0.131	0.114	0.128
US Research Nanomaterials Inc.	0.561	0.592	0.600	0.674	0.460	0.577
Nanostrucutred & Amorphous Matls.	0.537	0.539	0.533	0.538	0.538	0.537
SES Research	0.481	0.524	0.521	0.498	0.487	0.502
HELIX Material Solutions	0.792	0.475	0.597	0.487	0.758	0.620
IoLiTec	0.787	0.405	0.639	0.507	0.617	0.591
NanoCS	0.714	0.767	0.758	0.770	0.820	0.766
MKNano	0.604	0.584	0.601	0.557	0.579	0.585
Sigma-Aldrich	0.080	0.081	0.076	0.102	0.096	0.087
Nanoshel	0.762	0.974	0.829	0.807	0.721	0.819
Nanoshel Arc-Discharged	0.765	0.745	0.662	0.786	0.767	0.745
Ted Pella	0.898	0.898	0.853	0.857	0.833	0.858
General Nano	0.727	1.274	1.079	0.958	1.013	1.010
Pyrograf	0.205	0.237	0.062	0.167	0.165	0.167
Case Western University	0.447	0.483	0.408	0.493	0.522	0.470

Seven MWCNTs from four different sources were subjected to thermal conductivity measurements. These MWCNT samples include: one sample (from Pyrograf) provided by NASA, and one sample provided by a research group at Case Western University. All samples were measured in a temperature range between 150 K and 320 K. Seven MWCNT samples were further examined by our collaborators at the University of North Carolina at Charlotte using a Transmission Electron Microscope (TEM). The results of the Raman spectroscopy study, the derived thermal conductivities from the measurements, and TEM results of these samples with more detailed studies are presented below. The first sample that is presented is a MWCNT from General Nano which underwent a TEM study only. Next, the MWCNTs with low measured thermal conductivities (below 25 W/m-K) are presented followed by the samples with relatively high measured thermal conductivities. It is worth noting even the "high" thermal conductivities here are more than one order of magnitude lower than the expected values for CNTs (~3000 W/m-K or higher).

3.1 Samples for TEM Study Only

We performed a TEM study of a sample from General Nano. The sample underwent Raman spectroscopy that yield very high D/G ratio. The TEM study indicated a poor structure, and it was therefore decided that a thermal conductivity measurement was not required.

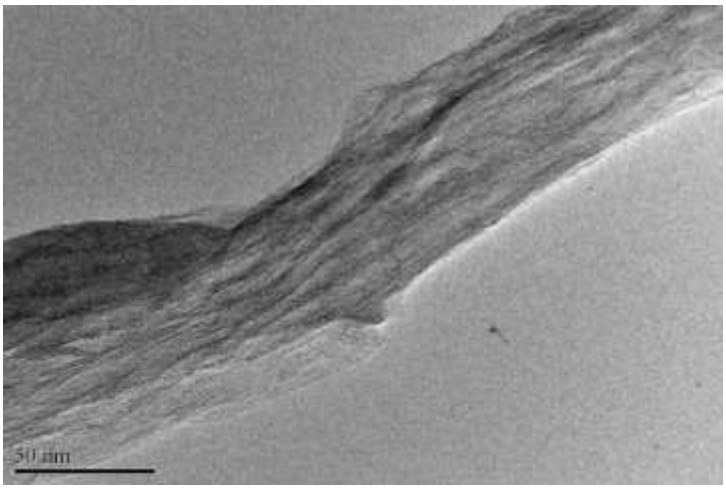

Figure 3.2- A TEM micrograph of a General Nano sample. The MWCNT does not have well defined diameter or wall thickness. The tube structure is not clear either.

Figure 3.2 shows a TEM image of a General Nano sample. It is easy to see that the carbon layers are not well ordered, and in fact, it is difficult to discern a clear tube structure. The diameter of the tube is not uniform and many defects are present. The wall thickness cannot be determined from the TEM analysis, nor can the amorphous layer thickness be calculated. Judging from the TEM pictures it was decided that a thermal measurement was not necessary, because the thermal conductivity is expected to be low based on the low quality of the tube structure.

3.2 Samples with Low Thermal Conductivities

3.2.1 MWCNTs from Sigma Aldrich

The first MWCNT that was found to have a very low thermal conductivity was purchased from Sigma Aldrich. This sample provided the best D/G ratio and therefore it

was assumed that the sample would have good thermal conductivity. **Table 3.3** gives the information gathered from the TEM study.

Table 3.3- TEM Results of a MWCNT from Sigma Aldrich

Position	Diameter (nm)	Wall Thickness (nm)	Amorphous Layer Thickness (nm)
1	~156.31	~76	~0.84
2	~170.68	N/A	~1.85
3	~235.5	N/A	~1.20

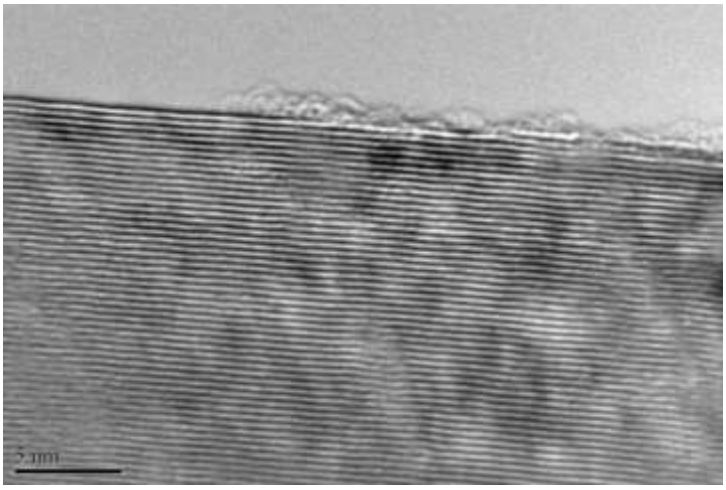

Figure 3.3- TEM image of Sigma Aldrich sample.

Figure 3.3 shows a TEM image of the Sigma Aldrich sample, which indicates clearly the aligned carbon tube layers. The tube is very thick and thus the wall thickness is hard to determine. Together with the low D/G ratio from the Raman spectroscopy analysis, we initially expected that the MWCNT sample could have a high thermal conductivity and thus conducted thermal conductivity measurement on one of the Sigma Aldrich sample.

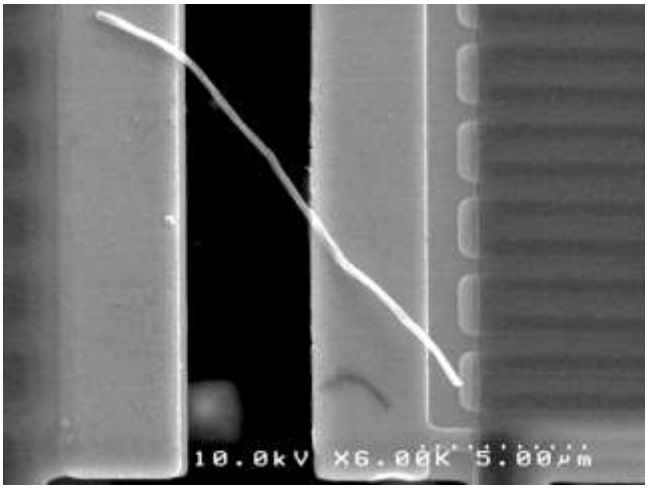

Figure 3.4- A Sigma Aldrich sample suspended on a measurement microdevice.

An SEM image of the measured sample on a measurement microdevice is shown in **Figure 3.4**, and this image was used to calculate the length of the tube suspended between the heating and sensing membranes. The suspended length was 6.45 µm, and from a high magnification image, the average diameter was determined as 239 nm. The large diameter of the sample in addition to the short contact length of the tube on each membrane could possibly lead to that the contact thermal resistance between the tube and the membranes significantly alter the derived thermal conductivity. However, the measured thermal conductivity is below 10 W/m-K, which is very low even consider the large diameter used to normalize the measured conductance. Therefore, no further study is extended to the Sigma Aldrich sample.

3.2.2 MWCNTs from Nanoshel

The next sample that was measured and showed a low thermal conductivity was produced by Nanoshel. This sample had a very poor D/G ratio; however it was claimed that the MWCNTs had a thermal conductivity of 2,400 W/m-K so we conducted a

thermal conductivity measurement. **Table 3.4** shows the information gathered from a TEM study.

Table 3.4- TEM Results of A CVD MWCNT from Nanoshel

Position	Diameter (nm)	Wall Thickness (nm)
1	~96.82	~39.5
2	~95.70	~41.56
3	~103.93	~47.60
4	~105.10	~49.35

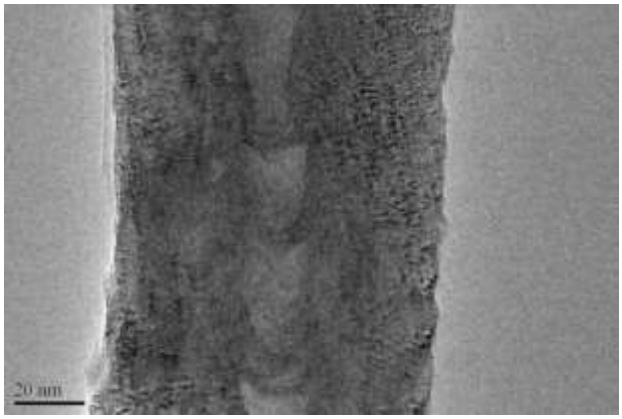

Figure 3.5- TEM micrograph of a Nanoshel sample. Amorphous carbon and defects can be clearly seen from the image, and the diameter is not well defined.

Figure 3.5 shows a TEM image of a Nanoshel MWCNT. It is apparent that there are many defects and that the tube is not of uniform diameter. In addition, the carbon layers seem not to form smooth concentric tubes, and in fact, it seems that the tube is really a herringbone CNT.

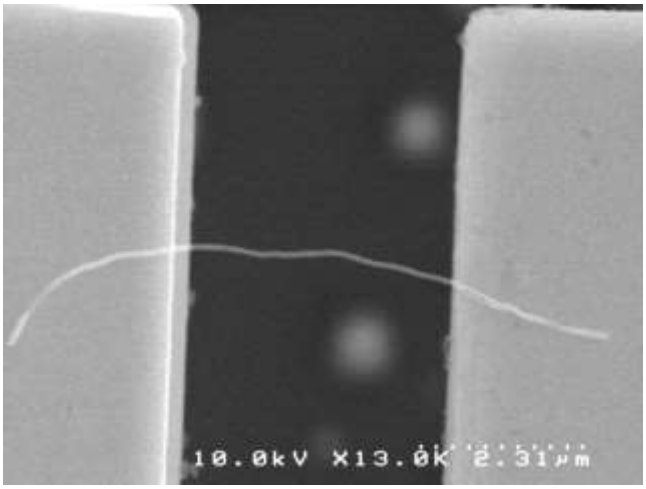

Figure 3.6- A Nanoshel CVD sample suspended on a microdevice.

Figure 3.6 depicts the suspended sample from Nanoshel. The suspended length was 4.2 µm. The diameter used in the thermal conductivity calculation was 131 nm. This sample did not have a long contact length with each membrane so the contact thermal resistance on each membrane may play a significant role in the measured thermal conductivity, especially considering the large diameter of the sample. However, since the measured thermal conductivity differed from the claimed thermal conductivity by two orders of magnitude and the TEM and Raman results were unimpressive we determined that these MWCNTs from Nanoshel could not provide us with the desired high thermal conductivities.

3.2.3 Nanoshel Arc Discharged

A sample grown by an arc-discharge method was acquired from Nanoshel and measured. While it is well known that generally MWCNTs prepared by the arc discharge method are of higher quality than samples grown by CVD, this was not the case for this sample. **Table 3.5** shows the results of the TEM study.

Table 3.5- TEM Results of A Nanoshel Arc-Discharge Sample

Position	Diameter (nm)	Wall Thickness (nm)
1	~62.9	~21.9
2	~52.4	~18.1
3	~49.8	~17.3

Figure 3.7 shows a TEM image of a Nanoshel Arc-Discharged sample. The tube is not of uniform diameter and there are many dislocations. The middle section is hollow; however the sample just barely resembles a cylinder. The sample does not consist of close packed cylinders of carbon that are necessary for good heat transfer characteristics.

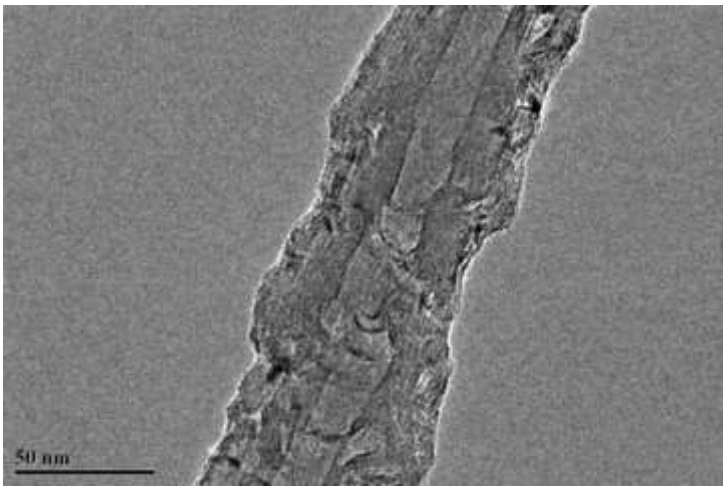

Figure 3.7- TEM image of Nanoshel Arc-Discharged sample. The sample is not uniform.

Figure 3.8 shows the Nanoshel arc-discharged sample on a microdevice. The suspended length is 3.17 μm, which is quite short. However, the tubes prepared by arc-discharge from Nanoshel did not have a long average length so to ensure that the contact thermal resistance on each membrane plays only a small role in the total thermal resistance, a microdevice with a small separation distance between the suspended membranes was used. The diameter of the sample averaged 131 nm, which may

introduce issues of relatively large contact thermal resistance. It is apparent that there are multiple surface defects and that the tube does not have a uniform cross section. This simple observation helps explain the extremely low thermal conductivity of the sample.

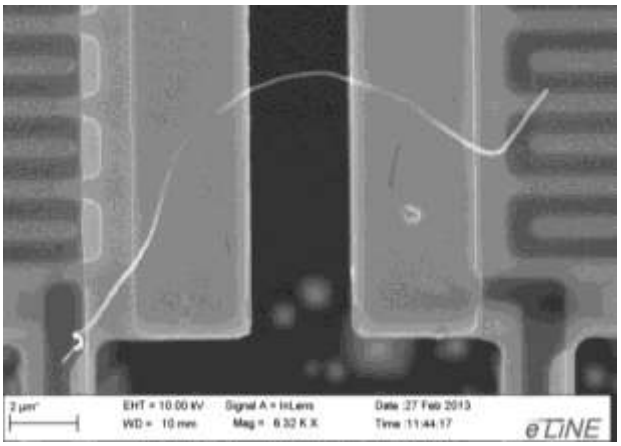

Figure 3.8- Nanoshel Arc-Discharged sample suspended on a microheater device.

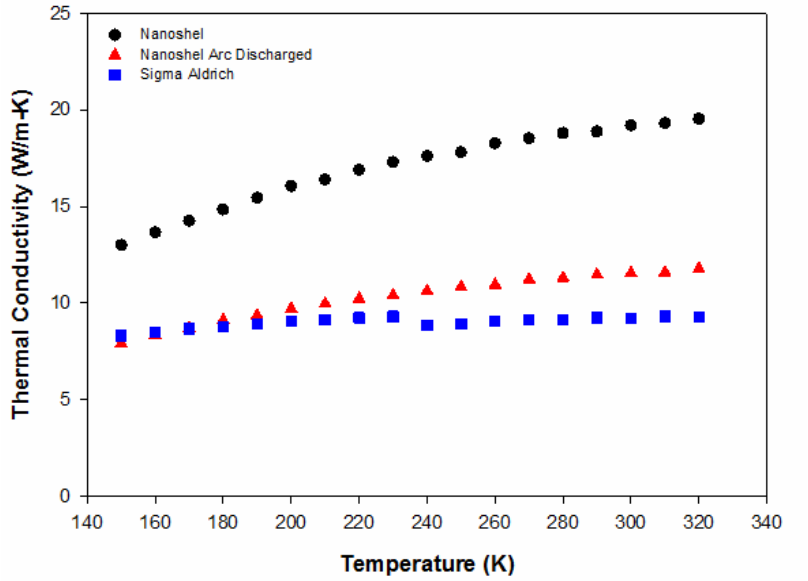

Figure 3.9- Thermal conductivity of samples with low thermal conductivities as a function of temperature. It is worth noting that these thermal conductivities are effective ones including the effects of contact thermal resistance between the MWCNT and the suspended membranes, which could be an important factor leading to the very low thermal conductivities.

The thermal conductivities as a function of temperature for the Sigma Aldrich sample, Nanoshel CVD sample, and the Nanoshel Arc-Discharged sample are shown in **Figure 3.9.** The peak thermal conductivity of the Sigma Aldrich sample is 9.32 W/m-K at 310 K. The peak thermal conductivity of the Nanoshel CVD sample is 13.01 W/m-K and the highest measured thermal conductivity of the Nanoshel Arc-Discharged sample is 11.79 W/m-K, with both of those peaks occurring at 320 K. We would like to emphasize that these extremely low thermal conductivities are likely due to that the contact thermal resistance dominance in the measurements of samples with very large diameters. However, the very low effective thermal conductivity suggests that even without the contact issue, the thermal conductivity cannot be very high, and is two orders of magnitude less than those values claimed in literature

3.3 Samples with Relatively High Thermal Conductivities

3.3.1 MWCNTs from Pyrograf

The first MWCNT sample that was measured for this study was a sample from Pyrograf provided by NASA. The sample was characterized using Raman spectroscopy, the thermal conductivity was measured, and a nanotube was studied using the TEM. The information gathered from the TEM study is shown in **Table 3.6**.

Table 3.6- TEM Results of the MWCNTs from Pyrograf

Position	Diameter (nm)	Wall Thickness (nm)	Amorphous Layer Thickness (nm)
1	~90.56	~25.06	~2.0
2	N/A	~22.56	~1.33
3	~87.49	~25.86	~1.29

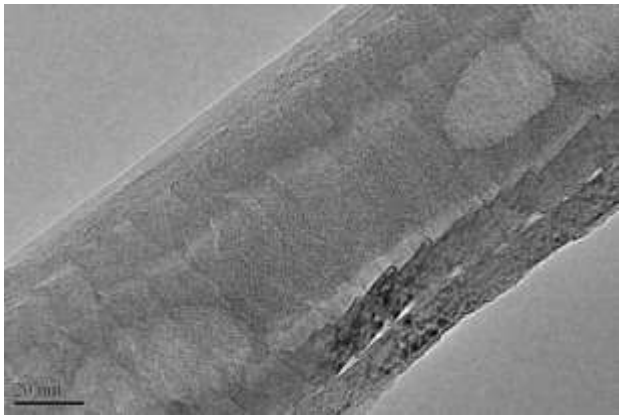

Figure 3.10- TEM image of a Pyrograf MWCNT sample.

Figure 3.10 shows a TEM image of a Pyrograf MWCNT. It is apparent that the tube is not of high quality and has many defects, which leads to enhanced phonon scattering and a low thermal conductivity.

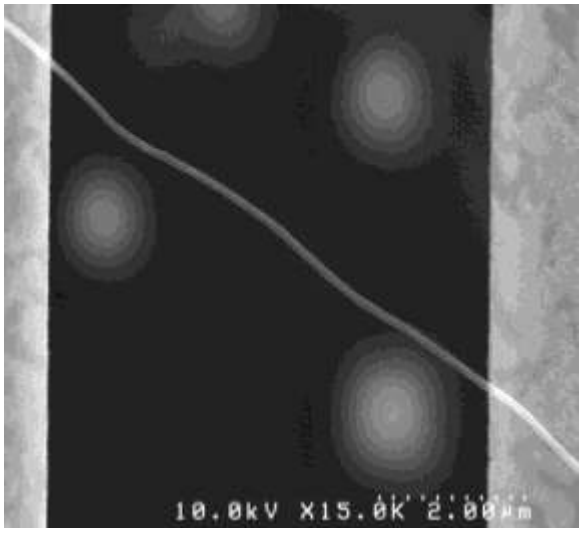

Figure 3.11- A Pyrograf MWCNT sample bridging the two suspended membranes on a microdevice.

Figure 3.11 shows an SEM image of the sample suspended between two membranes. The suspended length of this sample was 6.92 µm, the diameter of this

particular MWCNT was 80.6 nm as determined from an SEM image. The average D/G ratio of the sample was 0.167. This was the second lowest D/G ratio of all of the samples that we received.

3.3.2 Cheaptubes Graphitized

We received two samples from Cheaptubes. One sample was grown using Combustion Chemical Vapor Deposition and had poor Raman results. The other sample was produced using Catalyzed Chemical Vapor Deposition (CCVD) and Cheaptubes calls these MWCNTs "Graphitized Nanotubes." Cheaptubes claims that these MWCNTs have an electrical conductivity similar to that of graphite. **Table 3.7** shows the results of the TEM study.

Table 3.7- TEM Results of the MWCNTs from Cheaptubes

Position	Diameter (nm)	Wall Thickness (nm)	Amorphous Layer Thickness (nm)
1	~109.89	~43.62	~0.93
2	~116.43	N/A	~0.80
3	~79.94	~33.13	N/A

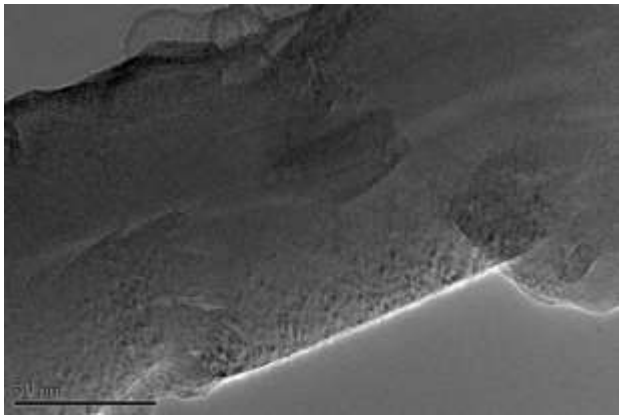

Figure 3.12- A TEM micrograph of a Cheaptubes Graphitized sample.

Figure 3.12 shows a TEM micrograph of the MWCNT from Cheaptubes. It is apparent that the tube is not perfectly cylindrical and has very little hollow space in the middle. Once again we expect that these defects could lead to enhanced phonon scattering, and hence a low thermal conductivity.

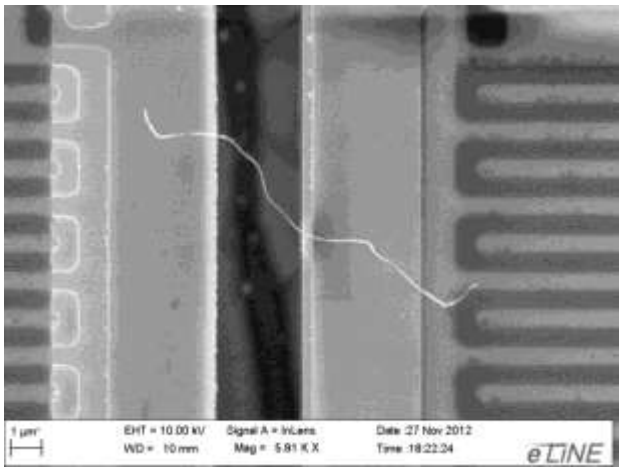

Figure 3.13- A Cheaptubes Graphitized sample placed between two suspended membranes on a measurement microdevice.

The sample that was measured is depicted in **Figure 3.13**. The suspended length was determined to be 4.61 µm and the average diameter was taken as 72 nm. The MWCNT had a highly irregular diameter making an accurate measurement difficult. The overall thermal transport characteristics of this sample were quite poor compared to values claimed in literature despite the promising Raman results. The low thermal conductivity most probably stems from the irregular diameter and poor structure of the MWCNT. Also, the contact length on the left side membrane is quite short, which means that the contact thermal resistance could be significant.

3.3.3 MWCNTs from Nanostructured & Amorphous Materials

One sample from Nanostructured & Amorphous Materials (NanoAmor) was measured because NanoAmor was established in 2001, making it one of the oldest MWCNT producing companies in existence. Because NanoAmor is an industry leader, we decided to perform a measurement on a sample from NanoAmor, despite the sample's average Raman results. No TEM study was performed; we simply measured the thermal conductivity and used those results to characterize the MWCNT.

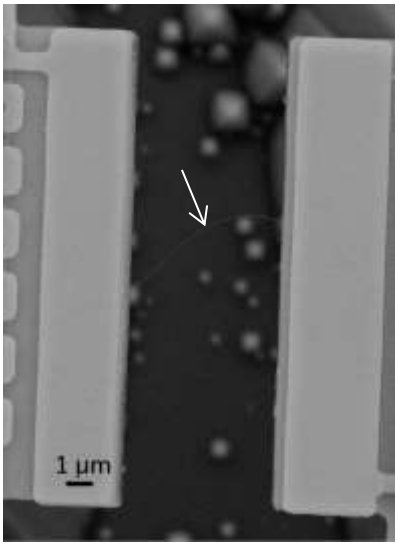

Figure 3.14- A NanoAmor MWCNT sample suspended on a microdevice

Figure 3.14 shows the sample placed on a microdevice. The suspended length was 7.53 µm, and the diameter was 52 nm. Because the MWCNT is in good contact with each membrane and the MWCNT has a relatively small diameter, contact thermal resistance should only play a small role in the measured thermal conductivity.

3.3.4 MWCNTs from the Case Western University

The final MWCNT that we analyzed came from a research group at Case Western University. The MWCNTs from this group had the best thermal properties. **Table 3.8** shows the results of the TEM analysis.

Table 3.8- TEM Results of MWCNTs from the Case Western University

Position	Diameter (nm)	Wall Thickness (nm)
1	~34.3	~9.1
2	~32.1	~10.2
3	~34.4	~10.1
4	~34.3	~8.2

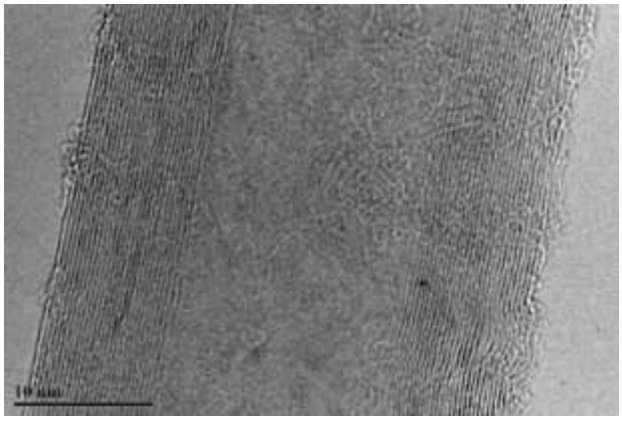

Figure 3.15- TEM image of the sample from Case Western University. The MWCNT is of very uniform diameter, with a few dislocations near the edges.

It is worth noting that for the Case Western sample the exact same MWCNT that was measured was placed on the TEM grid for inspection. A TEM image of the MWCNT is shown in **Figure 3.15**. The tube has a very uniform diameter and very little amorphous

carbon at the surface. The layers of carbon are mostly straight and well ordered, with a few dislocations present on the right side of the tube near the bottom. This particular MWCNT underwent a thermal measurement twice. In between the measurements the sample was manipulated to give a different suspended length between the membranes of the microdevice. From these two measurements the intrinsic thermal conductivity of the MWCNT could be extracted (Yang, 2011).

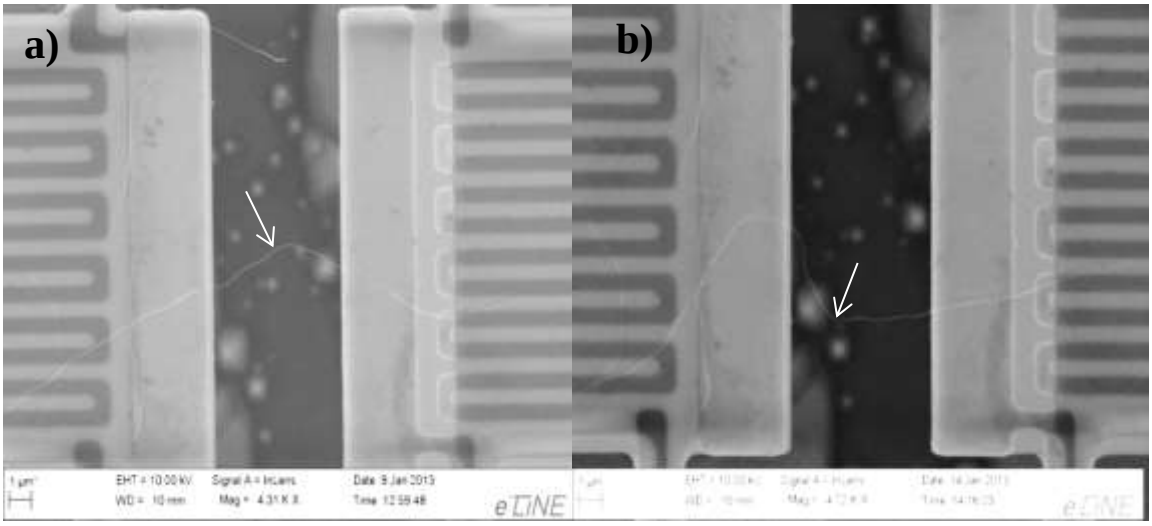

Figure 3.16- A MWCNT sample from Case Western University placed on a microdevice with a) 6.83 μm suspended length, and b) 8.37 μm suspended length.

The sample was first measured with a 6.83 μm suspended length as depicted in **Figure 3.16a**, and after the measurement, the sample was subjected to manipulation with the micromanipulator to have a suspended length of 8.37 μm between the two suspended membranes, as shown in **Figure 3.16b**. The sample was then measured again. Using the method outlined by Yang *et al.* (Yang, 2011), as briefly described in Chapter 2, the intrinsic thermal conductivity of the sample was derived.

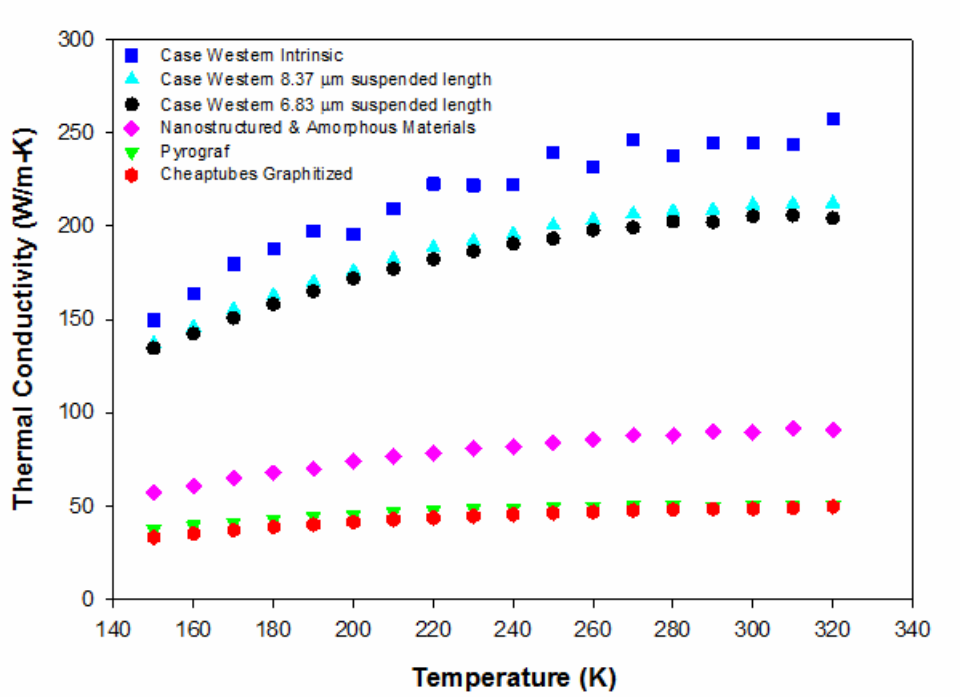

Figure 3.17- Thermal Conductivity vs. Temperature for samples with high thermal conductivities.

The thermal conductivities of the Pyrograf sample, the Cheaptubes Graphitized sample, the sample from NanoAmor and both measurements of the Case Western sample as well as the calculated intrinsic thermal conductivity are shown in **Figure 3.17**. The Pyrograf sample has a peak thermal conductivity of 50.66 W/m-K and the sample from NanoAmor has a peak thermal conductivity of 91.41 W/m-K. Both of those peak thermal conductivities are observed at 310 K. The Cheaptubes Graphitized sample peaks at 49.69 W/m-K at 320 K.

As mentioned earlier, the sample from Case Western was measured twice. For the first measurement the thermal conductivity ranged from 134.55 W/m-K at 150 K to 205.65 W/m-K at 310 K. The results from the second measurement when the suspended length was 8.37 µm were similar, however they were slightly higher. The results ranged

from 137.08 W/m-K at 150 K to 212.27 W/m-K at 320 K. This indicates that the contact thermal resistance on each membrane contributed to the thermal conductivity results. By subtracting the measured total thermal resistance from the two measurements, an intrinsic thermal conductivity was derived. The intrinsic thermal conductivity of the sample the thermal conductivity rose to 149.59 W/m-K at 150 K and a peak value of 257.35 W/m-K at 320 K. This is an increase of 9.1% at 150 K and 21.2% at 320 K. While this is a significant increase it is still far from the results that we desired for the thermal conductivity of a high quality MWCNT.

3.4 Summary

The study of structure quality and thermal conductivity of MWCNTs from different sources indicates that to have a high thermal conductivity, a good structure quality is required. Even though quite a few MWCNTs are examined, these CVD synthesized MWCNTs are in general of relatively low quality and their thermal conductivities are at most on the order of a couple hundreds of W/m-K, which is one order of magnitude lower than pristine SWCNTs or small diameter MWCNTs synthesized through arc discharged method. To better utilize the superior thermal properties of CNTs, high quality MWCNTs produced with strict quality control have to be readily available at large volume and low costs from the market.

Chapter 4

Thermal Transport through Gold Nanowires and Their Contacts

To date most thermal property measurements of 1-D nanostructures have been performed on samples in which phonons are the dominant energy carriers, such as carbon nanotubes (CNTs) and various semiconducting nanowires and nanoribbons. Much less attention has been paid to metallic nanowires in which electrons serve as the dominant energy carriers. In addition, metal nanoparticles and nanowires have been used to enhance the composite thermal conductivity (Patel, 2003). Therefore, we tried to measure the contact thermal resistance between individual gold nanowires using the approach developed by Yang *et al.* (Yang, 2011).

4.1 Gold Nanowire Contact Thermal Resistance

We set out to measure the thermal resistance of a point contact between two gold nanowires that are placed on a measurement microdevice in a crossed configuration. These measurements would then be compared to the measurement of a single gold nanowire to determine the thermal resistance of the point contact. A total of two measurements were performed with gold nanowires in a crossed configuration, and four more measurements were conducted with single nanowires.

Following the work done by Yang *et al*. as outlined in Chapter 1.3 of this thesis, we treat the total thermal resistance of a single measured nanowire as

$$R_{total} = R_{C-memb,l} + R_{wire/L} * L + R_{C-memb,r} \qquad 4.1$$

where $R_{C\text{-}memb,l}$ and $R_{C\text{-}memb,r}$ are the contact resistance with the left and right membranes, respectively. $R_{wire/L}$ is the thermal resistance of the suspended nanowire per unit length

and L is the suspended length between the membranes. If we then perform a measurement of nanowires in a crossed configuration the total thermal resistance can be written as

$$R_{total} = R_{C-memb,l} + R_{wire1/L} * L_1 + R_{C-wires} + R_{wire2/L} * L_2 + R_{C-memb,r} \quad 4.2$$

where $R_{wire1/L}$ is the thermal resistance of wire 1 per unit length and L_1 is the suspended length of wire 1 from the edge of the suspended membrane to the contact point. Similarly $R_{wire2/L}$ is the thermal resistance of wire 2 per unit length and L_2 is the suspended length of wire 2 from the contact point to the edge of the suspended membrane.

The contact thermal resistance between the two nanowires can be derived from Eq. 4.1 and Eq. 4.2 based on several assumptions. First, the contact thermal resistance between the wires and the membrane should be approximately the same for different measurements. In addition, the thermal resistance of the nanowires can be properly subtracted from the measured total thermal resistance.

Figure 4.1 shows the configuration of a sample with two gold nanowires forming a cross contact between the two suspended membranes. Both nanowires are ~80 nm in diameter and the total length of the heat transfer route between the two suspended membranes is about 7.5 μm. We conducted thermal measurement in a temperature range from 250 K to 350 K. The total length of the contact between the gold nanowires and the suspended membranes is 10.4 μm, with 6.1 μm of that contact occurring on the right side and 4.3 μm occurring on the left side.

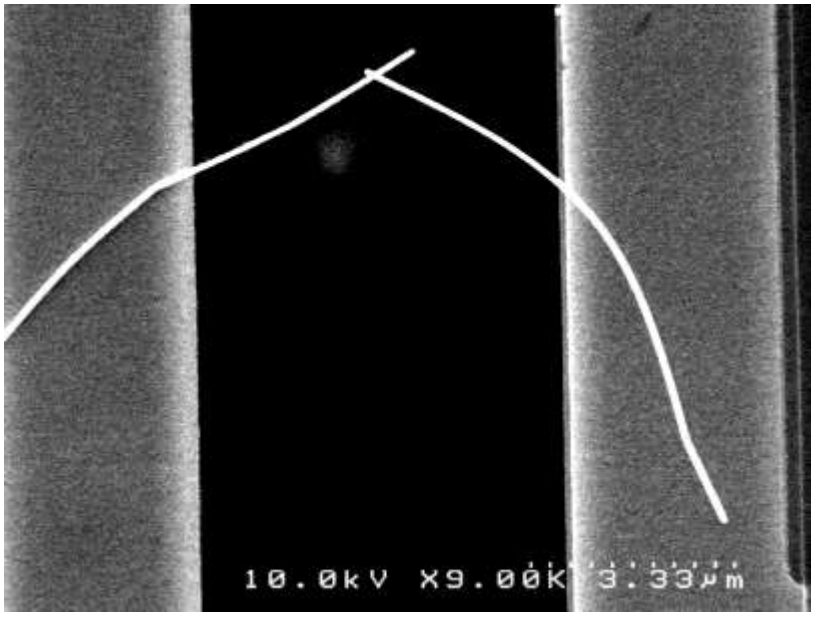

Figure 4.1 - A sample with two gold nanowires of ~80 nm diameter forming a cross contact.

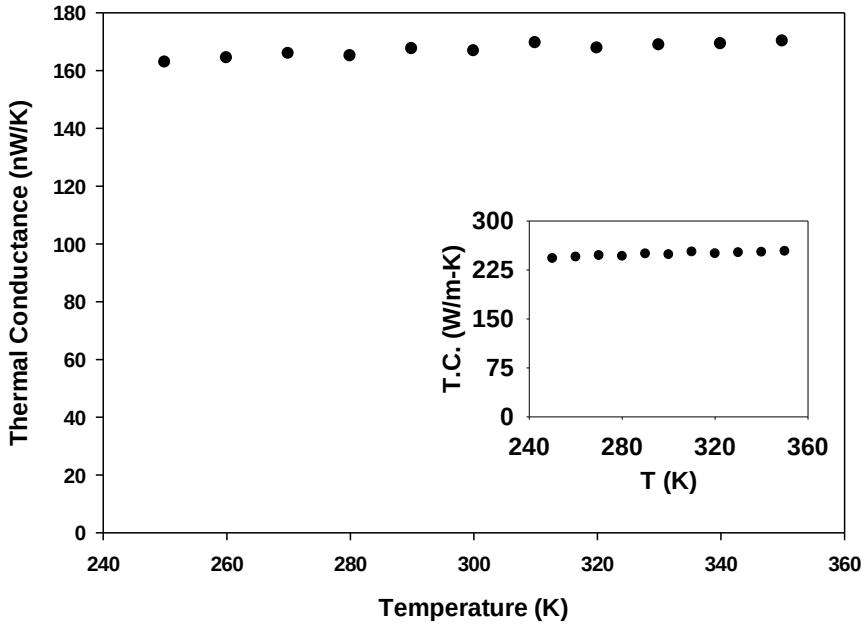

Figure 4.2- Measured total thermal conductance and nominal thermal conductivity of the sample with two ~80 nm diameter gold nanowires forming a cross contact.

Figure 4.2 shows the measured total thermal conductance of this sample. It can be seen that the total thermal conductance is approximately constant at about 170 nW/K. If we neglect the resistance from all the contacts and calculate a nominal thermal conductivity of the gold nanowire, a value of roughly 245 W/m-K is obtained, as shown in the inset of Fig. 4.2. It is worth noting that because of all the contacts, the derived nominal thermal conductivity should be less than the actual thermal conductivity of the gold nanowire. For comparison, the textbook value of thermal conductivity for bulk gold at 300 K is 318 W/m-K. As such, a value of 245 W/m-K represents 0.79 times the bulk thermal conductivity of gold. It is interesting to point out that this is much higher than that reported by Lu *et al*., which suggested a value of 0.35 for a gold nanowire of 80 nm width. This is especially true considering that this value includes the effects of contacts between the wire and the suspended membranes, as well as the small point contact between the two gold nanowires. From the case of MWCNTs, the resistance of the tiny point contact between two MWCNTs could contribute up to 40% of the total measured thermal resistance. However, for gold nanowires, the contact thermal resistance seems much smaller because if the contact thermal resistance is as significant as that for MWCNTs, then the thermal conductivity of the gold nanowires would be larger than that of the bulk gold, which is impossible.

Figure 4.3 shows a TEM micrograph of a gold nanowire. It can be seen that a thin amorphous layer exists on the outside of the gold nanowire. This amorphous layer ranges from less than 1 nm to about 3 nm. It is not clear what this amorphous layer is composed of and whether or not it was present on all of the wires. Gold is a noble metal and largely unreactive so the presence of this amorphous layer is quite surprising. It is worth noting

that there is a time gap of 7 months between the above discussed thermal measurement and the measurements described below. The TEM micrograph is taken about eight months after the samples were purchased and at this moment it is not clear whether this amorphous layer is due to surface adsorption during the long time storage period and whether it contributes to any difference between the measurements that were taken seven months apart.

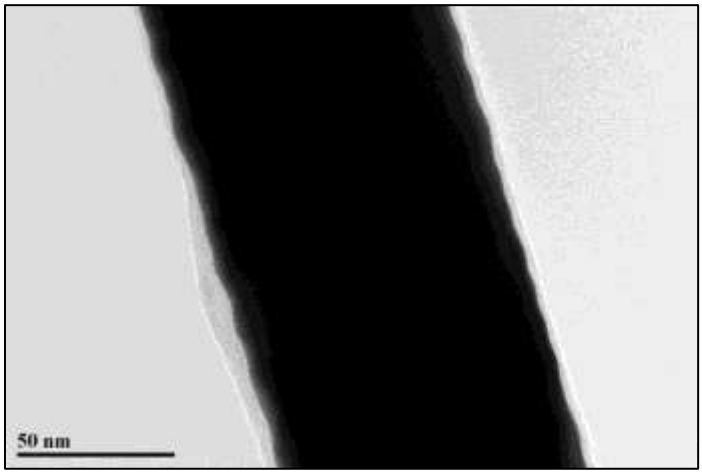

Figure 4.3 – A TEM micrograph of a gold nanowire.

Figure 4.4 depicts a sample with a cross contact between two gold nanowires of ~99 nm in diameter, which was subjected to thermal transport measurements. Based on SEM characterization, one wire has a diameter of 99 nm while the other has a diameter of 97 nm. An average of 98 nm was used for calculations. The suspended length of the crossed wires is 6.45 μm. The total contact length between the gold and the suspended membranes for this sample is 5.6 μm, with 2.2 μm of that contact occurring on the left side and 3.4 μm of that contact on the right side.

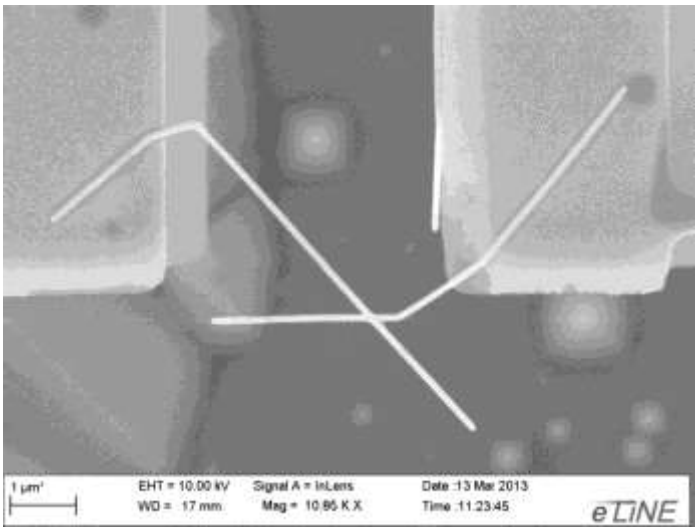

Figure 4.4 – A sample with two ~98 nm diameter gold nanowires forming a contact.

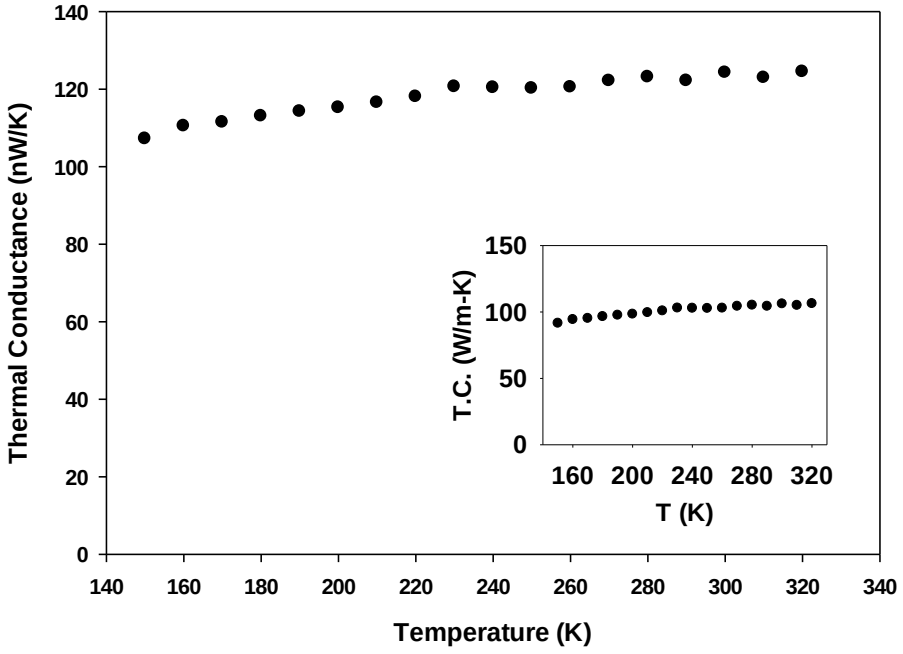

Figure 4.5- Measured total thermal conductance and derived nominal thermal conductivity of the sample with two ~98 nm diameter gold nanowires forming a cross contact.

Figure 4.5 shows the measured total thermal conductance and the derived nominal thermal conductivity of the sample composed of two ~98 nm diameter gold nanowires. The results show that the measured total thermal conductance is less than the sample with two ~80 nm diameter wires, which is not expected because we anticipated that larger diameter wire should have a higher thermal conductance. A couple of possible reasons could be responsible for this lower measured total thermal conductance. First, the contact length between the wire and the membrane is much smaller than that for the sample of ~80 nm diameter wires (it is worth noting that the contact length will be even smaller if the wire only makes good contact with the Pt on the suspended membranes but not the SiNx at the edges). Secondly, the amorphous layer, which could contribute more thermal resistance, might or might not exist on the ~80 nm diameter gold nanowires since they were prepared right after the samples were purchased. As a result of the lower measured thermal conductance, the derived nominal thermal conductivity is much lower than the previous sample, peaking at 106 W/m-K at 320 K.

The next step in determining the thermal resistance of the point contact between the two gold nanowires is to manipulate the nanowires to place one single gold nanowire between the two suspended membranes, which should have approximately the same suspended length as the heat transfer route in the sample with a cross contact. However, the manipulation was not successful so a good sample was not obtained with the gold nanowires in the cross-contact sample. It was therefore decided that a good solution was to find nanowires from the same dispersion (on the same piece of PDMS) with a similar diameter and determine the intrinsic thermal conductivity of those nanowires. The same process that was used to find the intrinsic thermal conductivity of a MWCNT from Case

Western University (Yang, 2011) was used for gold nanowires. This intrinsic thermal conductivity could then be used to calculate $R_{wire/L}$ in both Eq. 4.1 and Eq. 4.2. With this, if we can assume that the contact thermal resistances on each membrane are equal in different measurements we can then find the thermal resistance at the point contact between two gold nanowires. Two sets of measurements were carried out to find out the intrinsic thermal conductivity of a gold nanowire of ~100 nm diameter.

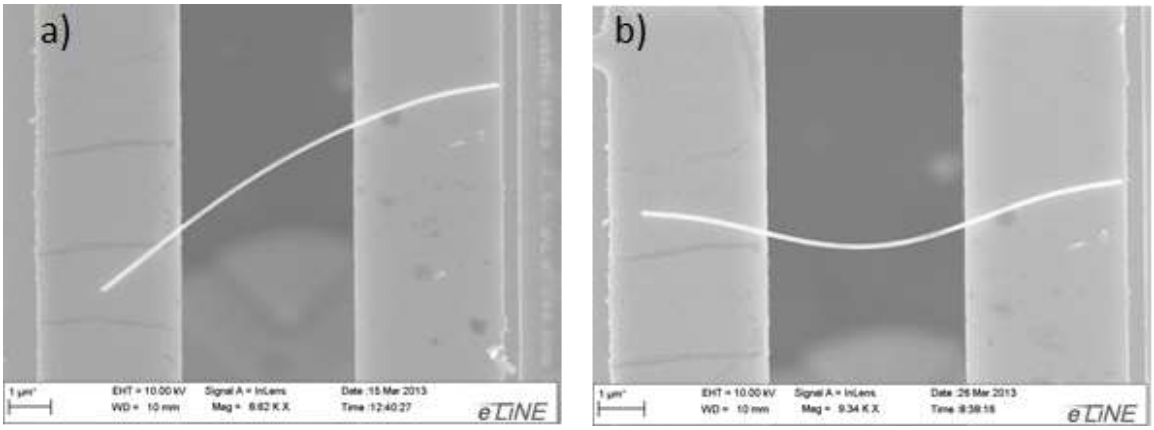

Figure 4.6 - First set of measurements of gold nanowire with different suspended lengths a) 4.86 μm b) 4.49 μm.

Figure 4.6 depicts the first two measurements carried out with the aim of finding the intrinsic thermal conductivity of a gold nanowire. The first measurement was carried out on a sample with a 4.86 μm suspended length and then the sample was manipulated to form a bridge across the two membranes and have a 4.49 μm suspended length. This corresponds to a change in suspended length of 7.6%. The diameter of this particular sample is 107 nm, which is 9.2% larger than the second crossed sample that was measured. In the first measurement the contact on the left side is 2.42 μm and the contact on the right side is 3.60 μm. The left and right contact lengths in the second measurement are 2.81 μm and 3.54 μm respectively.

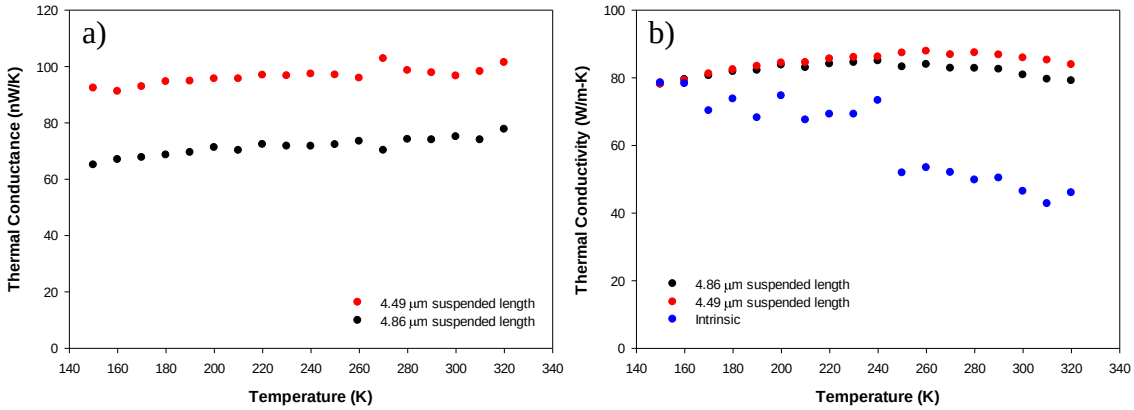

Figure 4.7- a) Measured thermal conductance and b) the extracted effective and intrinsic thermal conductivity of the ~107 nm diameter gold nanowire.

Figure 4.7 presents the measured total thermal conductance and the derived effective and intrinsic thermal conductivity utilizing the work of Yang, *et al.* (Yang, 2011). It can be seen that the total thermal conductance for the wire with shorter suspended length is higher, which seems reasonable because the total thermal resistance is lower. However, at temperatures higher than 170 K, the sample with the longer suspended length has a lower effective thermal conductivity, which is contradictory to the expectation. For the measurement scheme to be valid, the contact thermal resistance between the nanowire and the two suspended membranes needs to be approximately the same in different measurements. If this is the case, as the suspended segment becomes longer, the percentage of contact thermal resistance in the total measured thermal resistance gets smaller and the effective thermal conductivity should approach the intrinsic one, i.e., becomes higher instead of lower. Now limited by the short length of the gold nanowire, the contact length on the left side membrane in the first measurement is only 2.42 μm and in the second measurement it increases to 2.81 μm. It is highly possible

that this short contact length is not enough for the nanowire to become fully thermalized with the suspended membrane. As a result, the contact thermal resistance varies in these two measurements, which leads to the unreasonable results of a lower intrinsic thermal conductivity than the effective one.

Another sample was prepared for measurements with longer contacts on each membrane. The sample also had a smaller diameter and between measurements the suspended length was changed by a larger amount. Because the gold nanowires are only a maximum of ~10 μm in length a microheater with a separation of 3 μm between membranes was used. The goal of using a device with such a small separation distance was to maintain long contacts on each membrane while also having the freedom to manipulate the gold nanowire and obtain significantly different suspended lengths.

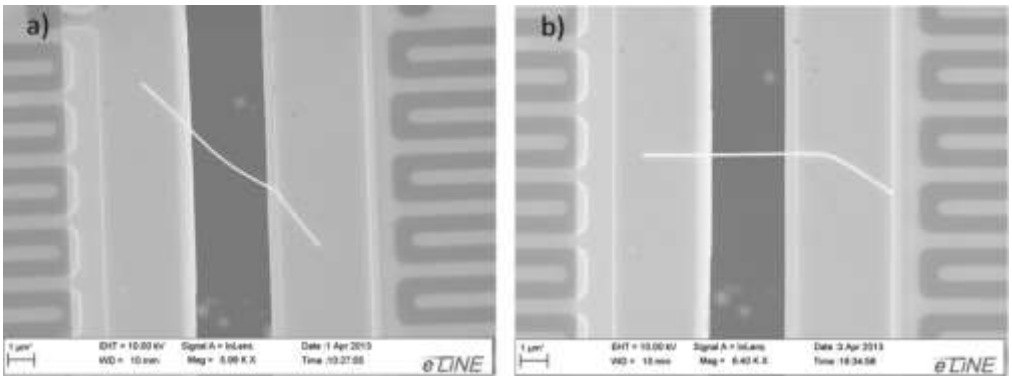

Figure 4.8 - Second set of measurements of gold nanowire with different suspended lengths a) 4.07 μm b) 3.00 μm.

Figure 4.8 shows the second measurement that was carried out in order to determine the intrinsic thermal conductivity of a gold nanowire. The first measurement was carried out on a sample with a 4.07 μm suspended length and then the sample was

manipulated to form a bridge across the two membranes and have a 3.00 µm suspended length. This corresponds to a change in suspended length of 26%. This sample has a diameter of ~103 nm, which is much closer to the diameter of the sample composed of two ~98 nm diameter wires with a cross-contact that we measured. The contact lengths were 2.7 µm on both sides for the first measurement, and the contact length was 2.5 µm on the left side and 4.0 µm contact length on the right side for the second measurement.

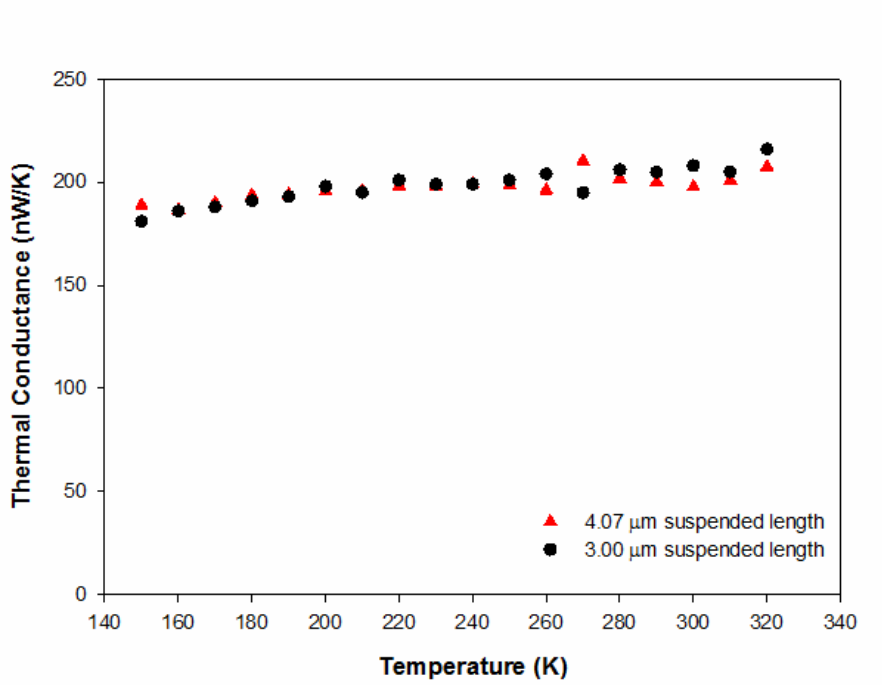

Figure 4.9- Measured thermal conductance of the ~103 nm diameter gold nanowire sample.

The measured sample thermal conductance changed very little at each temperature point between the two measurements, even though the suspended length changed by 26%. Also, the change in measured thermal conductance does not follow a consistent trend. At some temperatures the measured conductance of the sample with a longer suspended length is higher, and at other temperatures it is lower. Most probably

this is because when the sample is manipulated to have a shorter suspended length, the wire is not fully in contact with the suspended membranes. Therefore the wire does not actually have contact lengths of 2.5 μm and 4.0 μm, but much shorter contact lengths.

Instead of attempting to use the simple model that was used in an attempt to analyze the last set of measurements, we used the fin model outlined in Yang *et al.* (Yang, 2011) to try to calculate the contact thermal resistance per unit length between the nanowire and the membranes. We hoped that this would allow us to determine the intrinsic thermal resistance of the nanowire, even if the contact thermal resistance is dominating the thermal measurement. Using this model with two measurements of the same gold nanowire we can find that

$$R_{Total1} = \frac{2\sqrt{R_{Au/L} \cdot R_C}}{\tanh(L_{C1}\sqrt{R_{Au/L}/R_C})} + R_{Au/L} * L_1 \qquad 4.3$$

$$R_{Total2} = \frac{2\sqrt{R_{Au/L} \cdot R_C}}{\tanh(L_{C2}\sqrt{R_{Au/L}/R_C})} + R_{Au/L} * L_2 \qquad 4.4$$

where $R_{Au/L}$ is the intrinsic thermal resistance per unit length, and R_C is the contact thermal resistance per unit length. L_{C1} and L_{C2} are the contact lengths between the nanowire and the membranes for the first measurement and the second measurement respectively. L_1 and L_2 are the suspended lengths of the nanowire for the first measurement and second measurement respectively. Using these two equations we have two unknowns ($R_{Au/L}$ and R_C) and two equations. We attempt to solve these two equations simultaneously using MATLAB software. This approach was first validated using data gathered from the measurements of Case Western MWCNTs. The MWCNTs had a very long contact length with each membrane, and therefore $L_C\sqrt{R_{Au/L}/R_C} >> 2$. This method

also proved valid because the sample from Case Western had such a small diameter. This means that the percentage of the thermal resistance due to contacts with each membrane is relatively small compared to the intrinsic thermal resistance of the tube. Using this newly developed MATLAB code we obtained the same results for the intrinsic thermal conductivity as discussed in Chapter 3.

However, when this method was applied to gold nanowires the results that we obtained were very scattered and did not show a consistent trend, even yielding a negative intrinsic thermal conductivity at some temperature points. The possible reason for this failure could be as follows.

First, this model only takes into account the total contact length between the nanowire and both membranes. However, if the nanowire has a much longer contact length on one membrane then the contact thermal resistance between the nanowire and the membrane with the shorter contact will dominate. For example, in one measurement the nanowire had a contact length of 2.5 μm on one side and 4.0 μm on the other.

Another issue with the measurements is that the gold nanowires have relatively large diameters (~100 nm) and short contact lengths (~2-4 μm on each side). Because the intrinsic thermal resistance of the nanowire scales with $1/r^2$ and the contact thermal resistance approximately scales with $1/l$, for a successful measurement smaller diameter wires are needed and/or longer wires that can become fully thermalized with the membranes. It appears that for the gold nanowire measurements that were conducted and reported in this thesis the contact thermal resistance accounts for a very large percent of the contact thermal resistance. In the measurements of the MWCNT from Case Western University the contact thermal resistance accounted for about 55-65%. If longer and

thinner wires can be obtained and placed on measurement devices so that the contact thermal resistance accounts for only 40-50%, then good results can be obtained.

4.2 Summary

The study of contact thermal resistance between two individual gold nanowires as well as single gold nanowires did not yield expected results because the contact thermal resistance between the wires and the suspended membranes plays a significant role or even dominate the total measured thermal resistance. Interestingly, the nominal thermal conductivity of the ~80 nm diameter gold nanowires, even with effects of all the contact thermal resistance, could be 245 W/m-K at 300 K, about 80% of the thermal conductivity of bulk gold, which is different from theoretical prediction in the literature for metal.

Chapter 5

Conclusions

The work that has been completed for this thesis has led to some interesting results. In this chapter we summarize the results and discuss their implications. In general, we have studied the thermal conductivity of multi-walled carbon nanotube (MWCNT) samples from different sources as well as thermal transport through individual single gold nanowires and gold nanowires with a cross contact.

5.1 Multi-walled Carbon Nanotubes

It seems to us from the majority of our thermal conductivity measurements that most CVD MWCNTs readily available in large volume are of relatively low quality. Published literature claims that single-wall carbon nanotubes (SWCNTs) can have a thermal conductivity up to 6,600 W/m-K (Berber, 2000), and MWCNTs can have a thermal conductivity higher than 3,000 W/m-K (Kim, 2001; Pop, 2006). However, the highest thermal conductivity that we obtained is merely 257.35 W/m-K from a sample produced by Case Western University. The measured effective thermal conductivities of commercially available MWCNTs ranged from 9.32 W/m-K to 91.41 W/m-K. It is worth noting that these low values are effective thermal conductivities including the effects of contact thermal resistance in the measurements. However, we estimate that removing the contact thermal resistance will only lead to thermal conductivities of a couple of hundreds W/m-K, still far below the claimed very high thermal conductivities for MWCNTs. This study strongly suggest that in engineering practice such as using CNTs to enhance the thermal conductivity of CNT-based composites, it cannot be blindly

assumed that CNTs have very high thermal conductivity. This is because thermal properties of MWCNTs are highly dependent on their physical structure and our Raman spectroscopy examination and TEM characterization indicate that many bonding and structural defects exist in these MWCNTs. In the future it may be helpful to study smaller MWCNTs and MWCNTs produced by various methods, including more samples produced by arc discharge method.

5.2 Gold Nanowires

We set out to extract the thermal resistance of a point contact between two gold nanowires. Two measurements were made each with two gold nanowires forming a cross contact. Interestingly, one measurement indicated a surprisingly high nominal thermal conductivity even with the effects of all contact thermal resistance. However, the other one did not, most probably due to the short contact length between the nanowire and the two suspended membranes.

After these two measurements of gold nanowires with contacts, we attempted to derive the intrinsic thermal conductivity of a single gold nanowire by measuring the same wire twice with different suspended lengths. However, because the available nanowires were relatively short and it turned out that the contact between the nanowires and the suspended membranes could contribute significant thermal resistance if the contact length was short, the attempts were not successful. As such, the contact thermal resistance between two gold nanowires could not be derived. However, these attempts indicate that in continuing this line of research, longer and thinner gold nanowires are needed to reduce the percentage of the thermal resistance due to contact with the membranes.

Appendix A

Raman Results

A.1 Cheaptubes

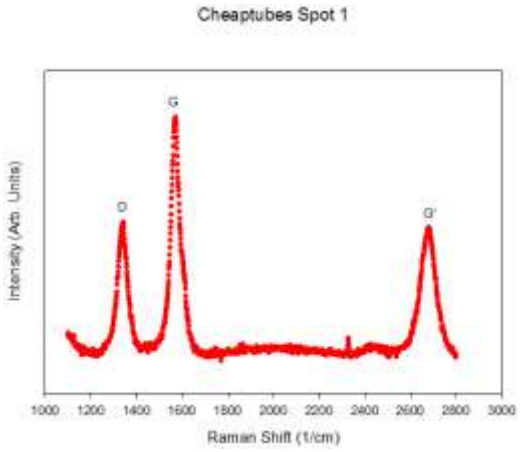

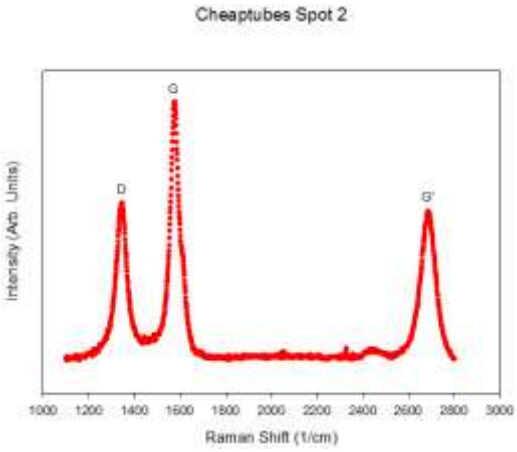

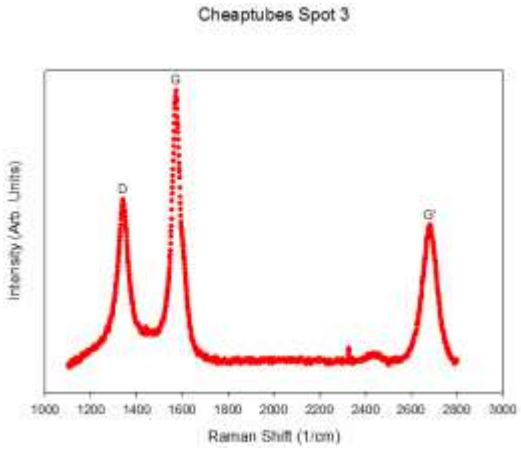

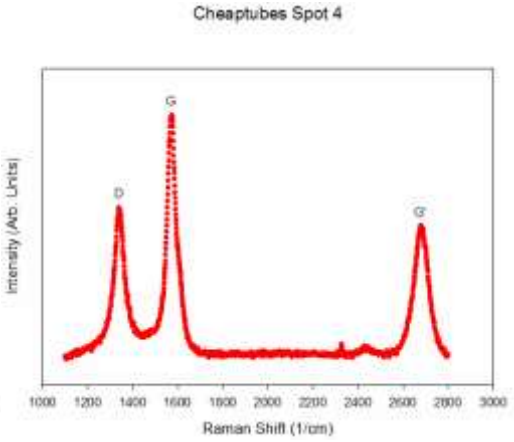

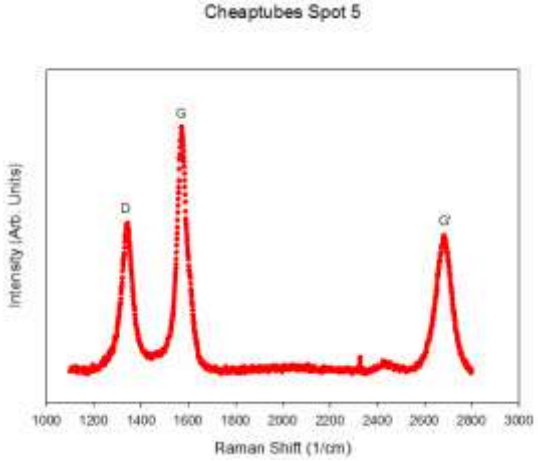

A.2 Cheaptubes Graphitized

Cheaptubes Graphitized Spot 1

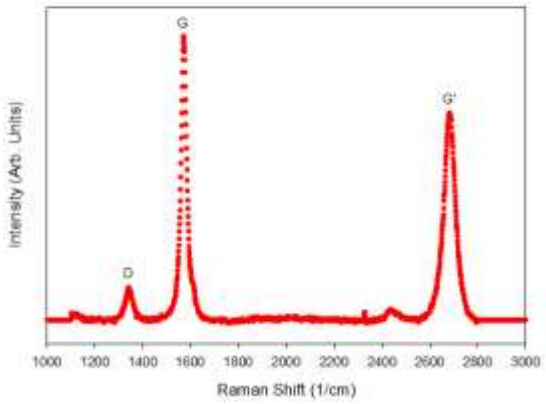

Cheaptubes Graphitized Spot 2

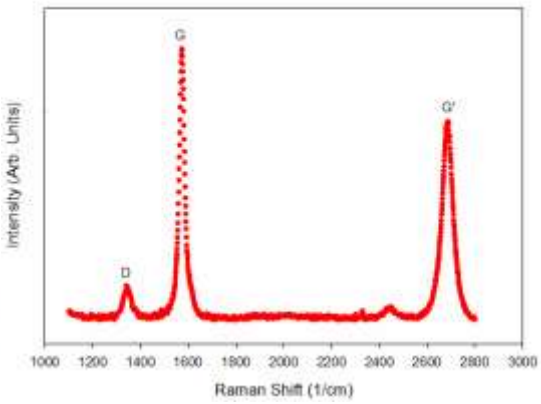

Cheaptubes Graphitized Spot 3

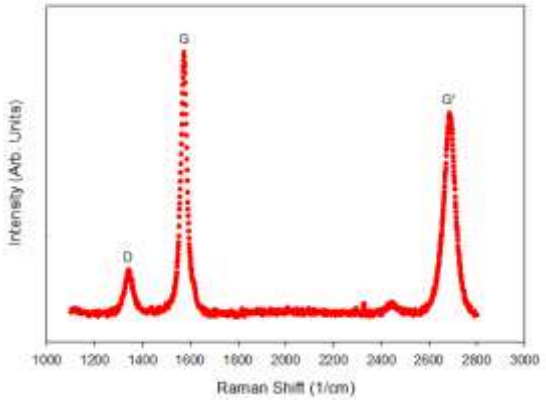

Cheaptubes Graphitized Spot 4

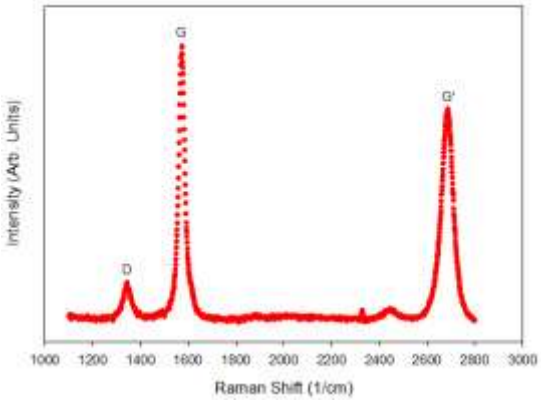

Cheaptubes Graphitized Spot 5

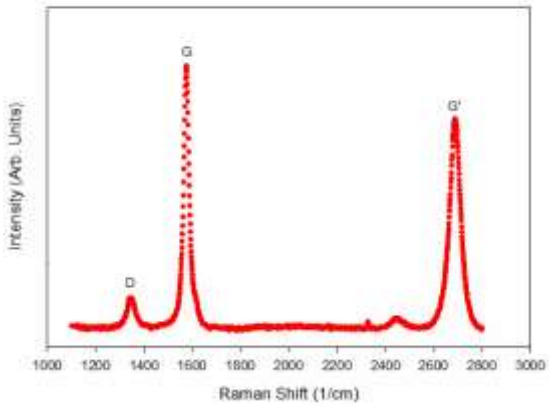

A.3 US Research Nanomaterials Inc.

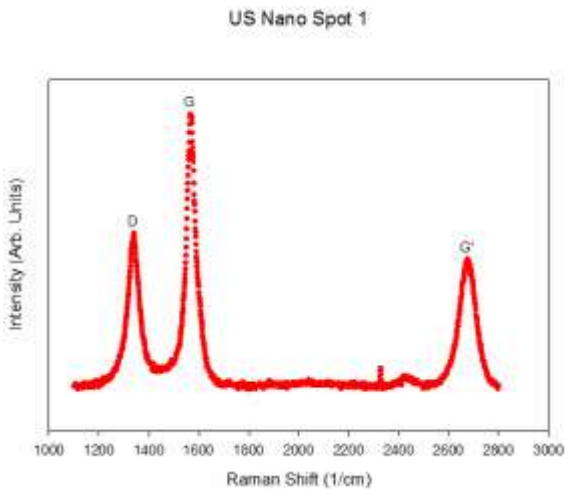

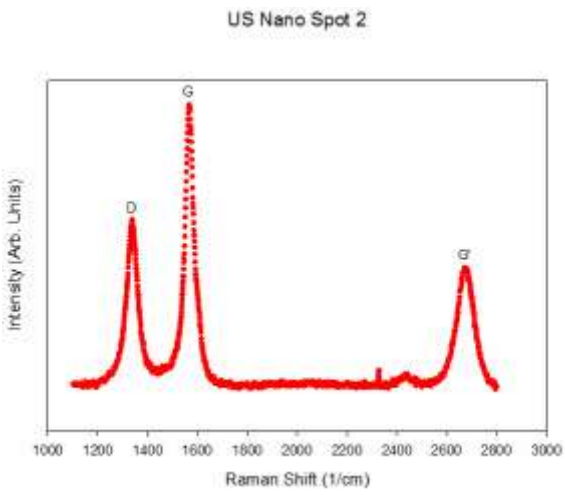

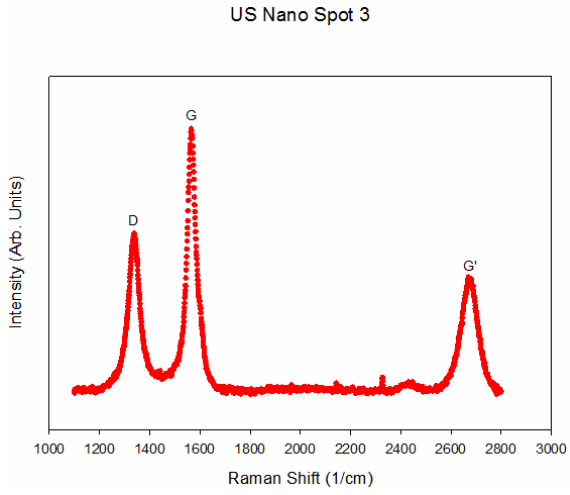

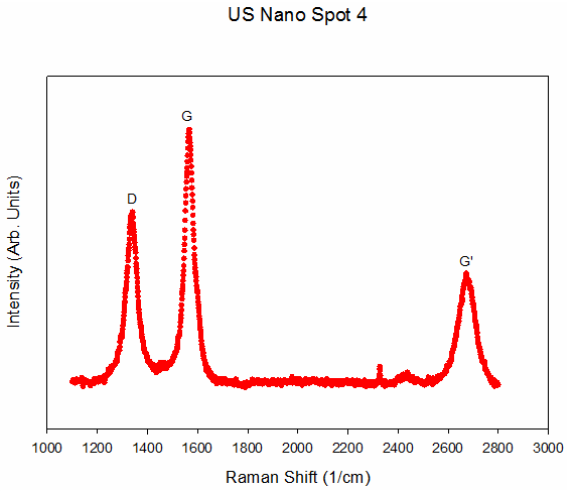

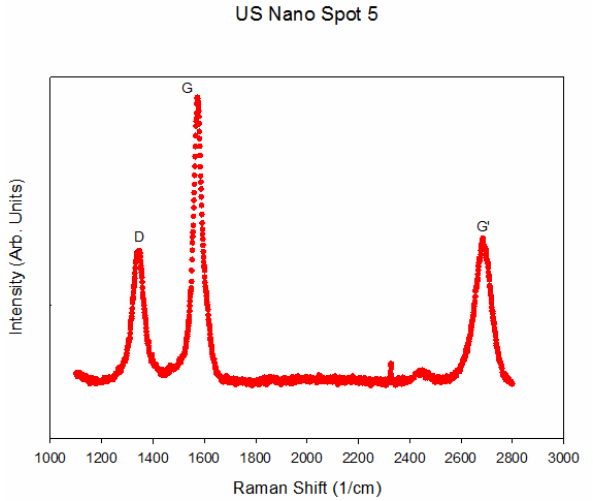

A.4 Nanostructured & Amorphous Materials

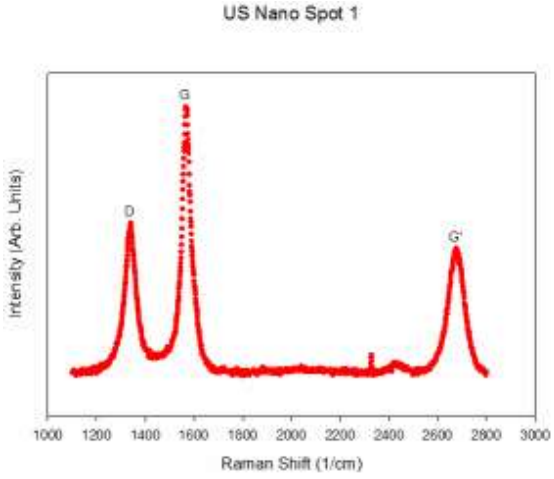

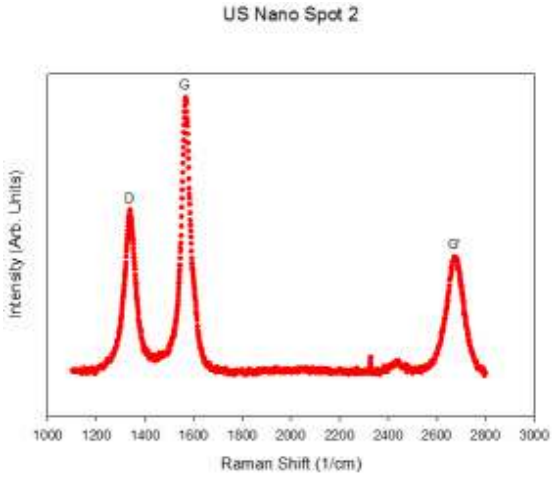

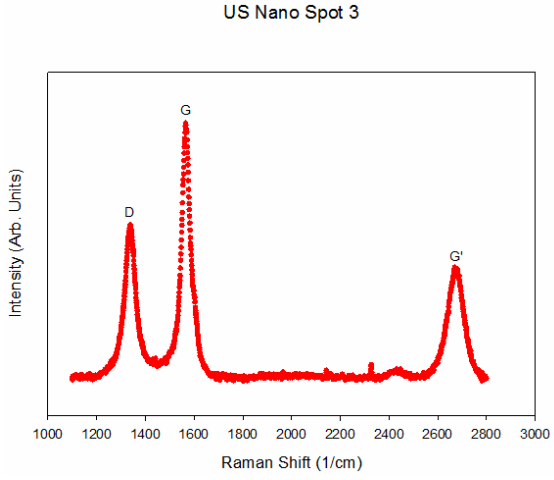

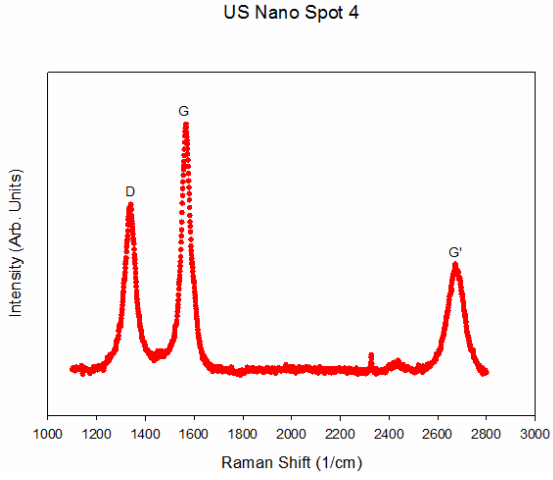

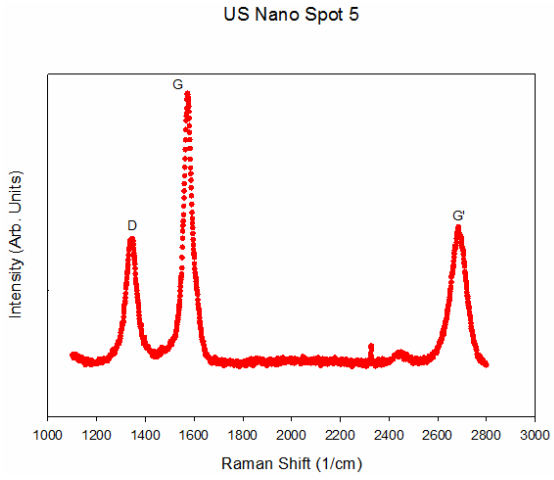

A.5 SES Research

SES Research Spot 1

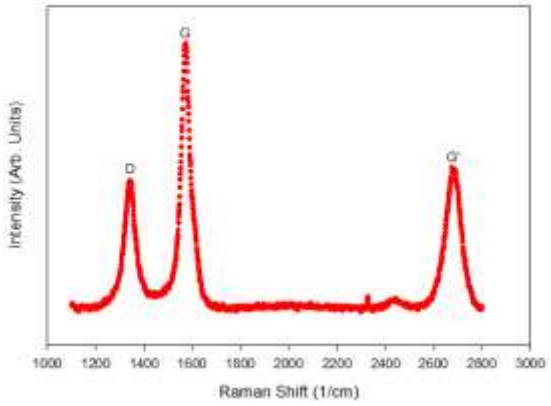

SES Research Spot 2

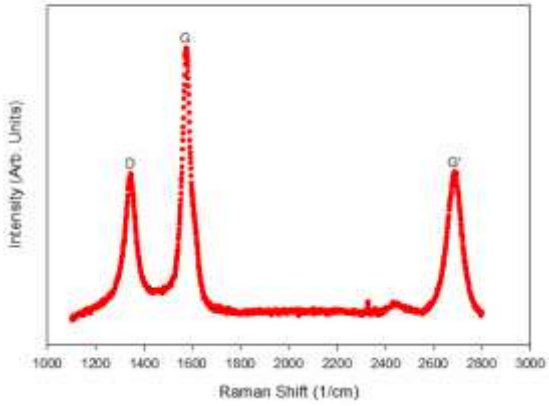

SES Research Spot 3

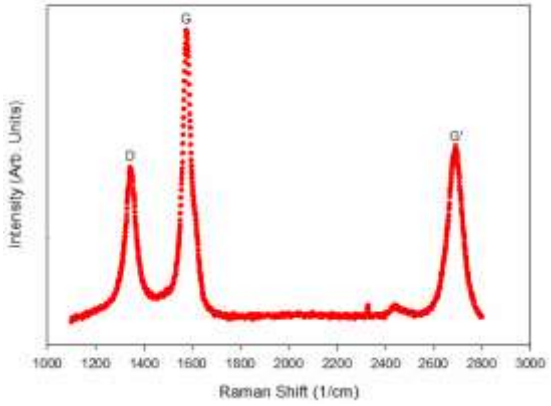

SES Research Spot 4

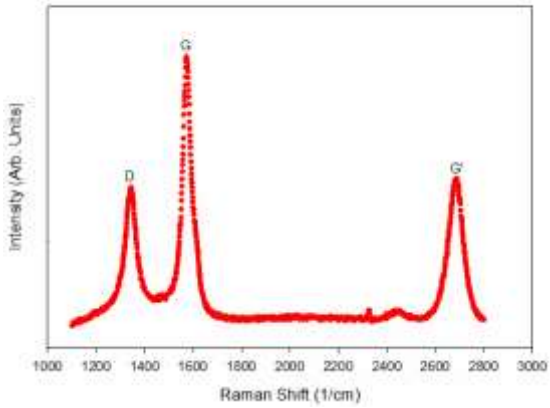

SES Research Spot 5

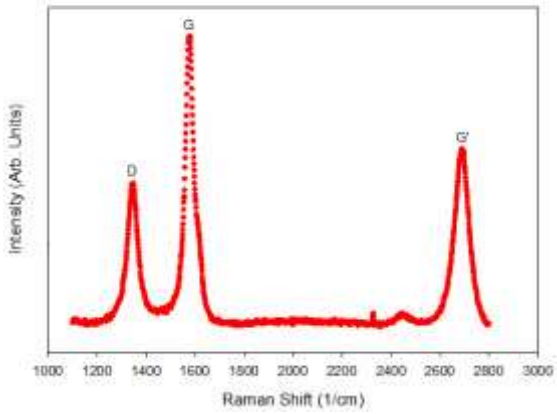

A.6 HELIX Material Solutions

HELIX Spot 1

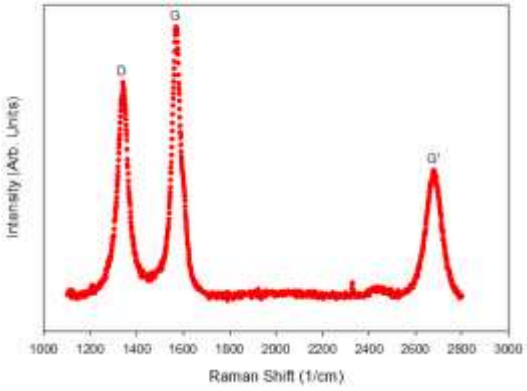

HELIX Spot 2

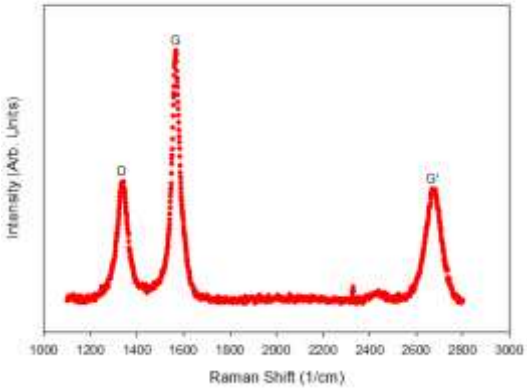

HELIX Spot 3

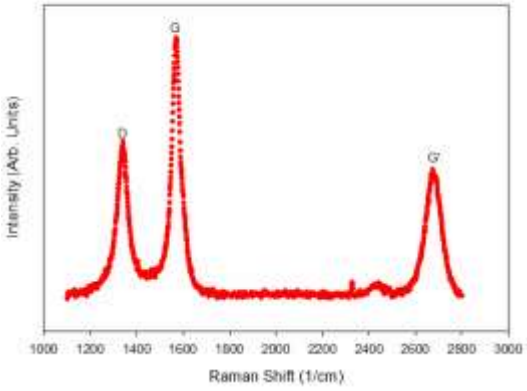

HELIX Spot 4

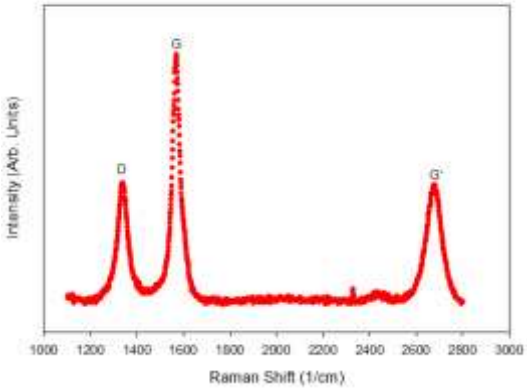

HELIX Spot 5

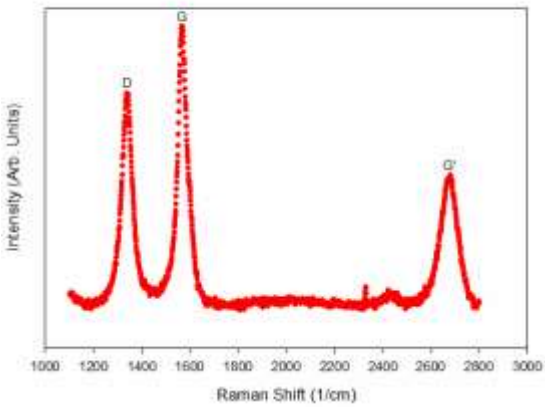

A.7 IoLiTec

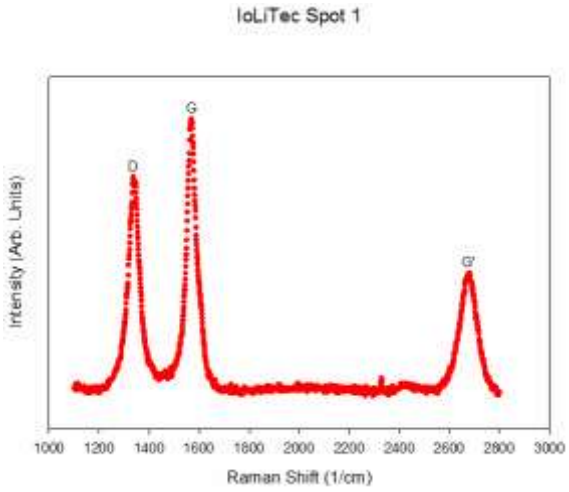
IoLiTec Spot 1
Intensity (Arb. Units)
D
G
G'
1000 1200 1400 1600 1800 2000 2200 2400 2600 2800 3000
Raman Shift (1/cm)

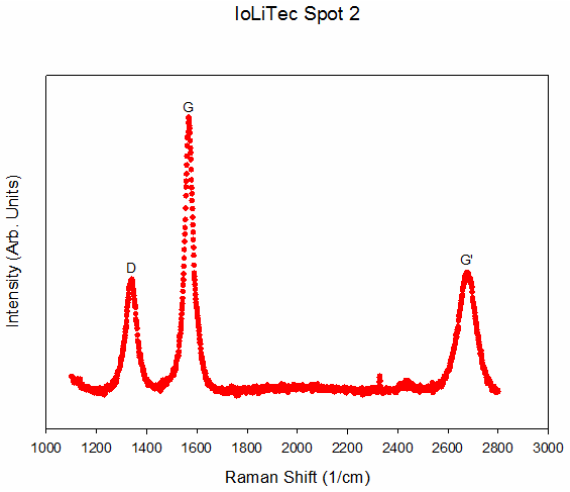
IoLiTec Spot 2
Intensity (Arb. Units)
D
G
G'
1000 1200 1400 1600 1800 2000 2200 2400 2600 2800 3000
Raman Shift (1/cm)

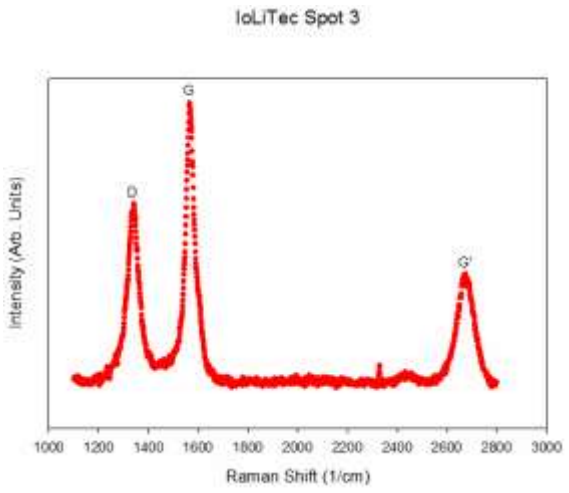
IoLiTec Spot 3
Intensity (Arb. Units)
D
G
G'
1000 1200 1400 1600 1800 2000 2200 2400 2600 2800 3000
Raman Shift (1/cm)

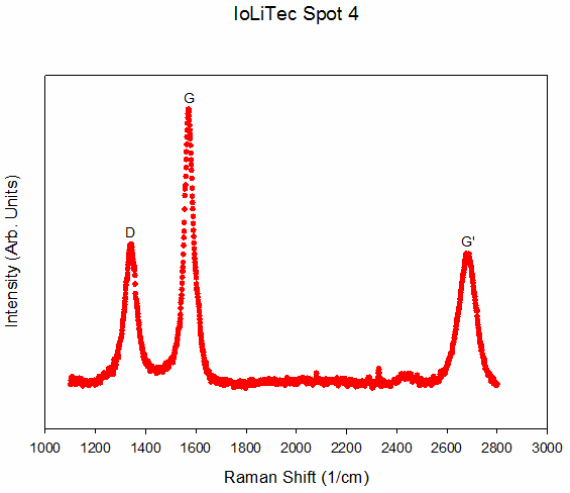
IoLiTec Spot 4
Intensity (Arb. Units)
D
G
G'
1000 1200 1400 1600 1800 2000 2200 2400 2600 2800 3000
Raman Shift (1/cm)

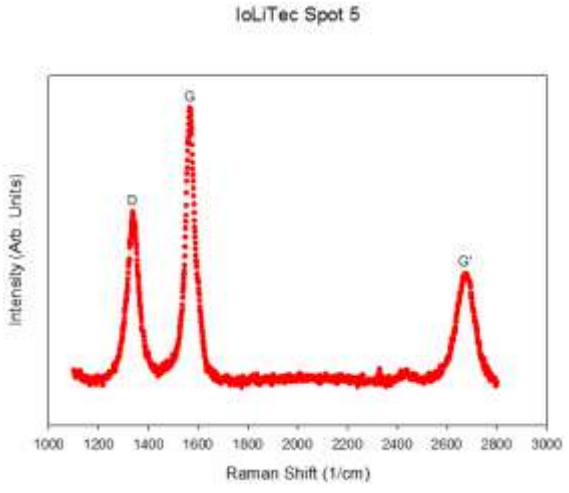
IoLiTec Spot 5
Intensity (Arb. Units)
D
G
G'
1000 1200 1400 1600 1800 2000 2200 2400 2600 2800 3000
Raman Shift (1/cm)

A.8 Nano CS

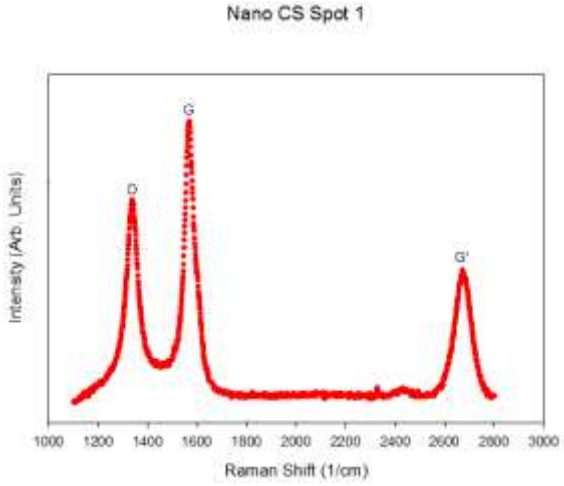
Nano CS Spot 1
Intensity (Arb. Units)
D
G
G'
1000 1200 1400 1600 1800 2000 2200 2400 2600 2800 3000
Raman Shift (1/cm)

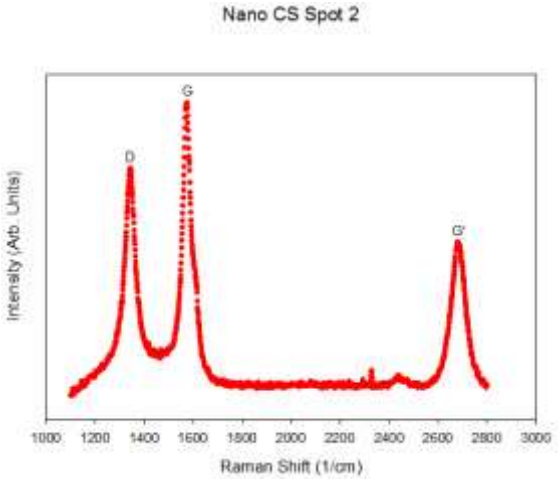
Nano CS Spot 2
Intensity (Arb. Units)
D
G
G'
1000 1200 1400 1600 1800 2000 2200 2400 2600 2800 3000
Raman Shift (1/cm)

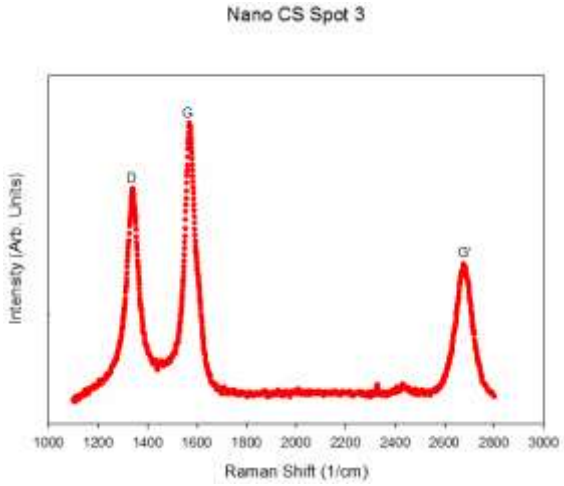
Nano CS Spot 3
Intensity (Arb. Units)
D
G
G'
1000 1200 1400 1600 1800 2000 2200 2400 2600 2800 3000
Raman Shift (1/cm)

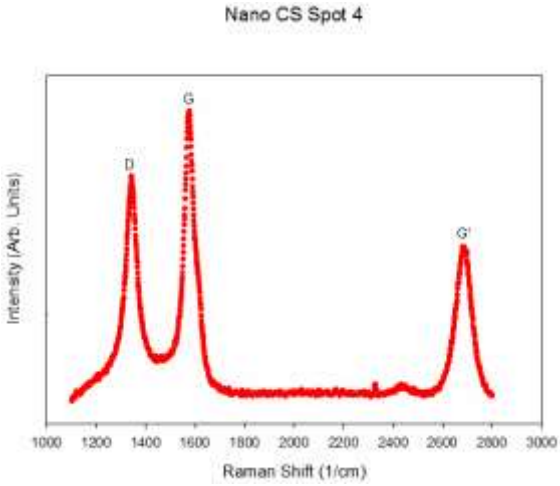
Nano CS Spot 4
Intensity (Arb. Units)
D
G
G'
1000 1200 1400 1600 1800 2000 2200 2400 2600 2800 3000
Raman Shift (1/cm)

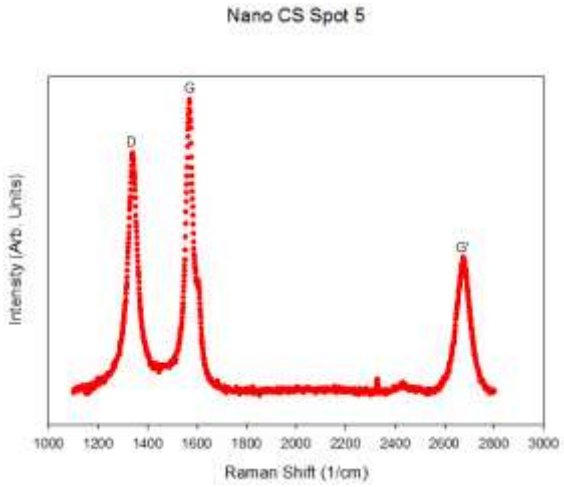
Nano CS Spot 5
Intensity (Arb. Units)
D
G
G'
1000 1200 1400 1600 1800 2000 2200 2400 2600 2800 3000
Raman Shift (1/cm)

A.9 MKNano

MKNano Spot 1

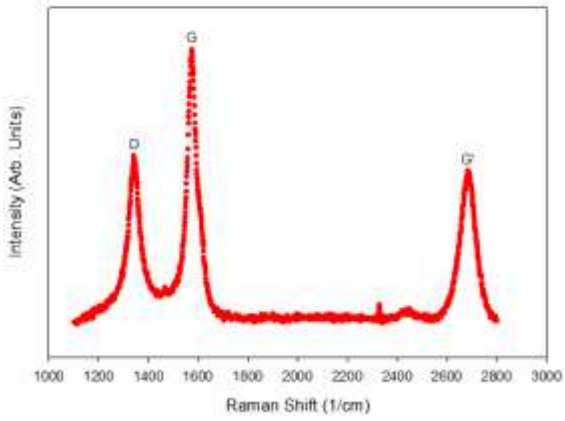

MKNano Spot 2

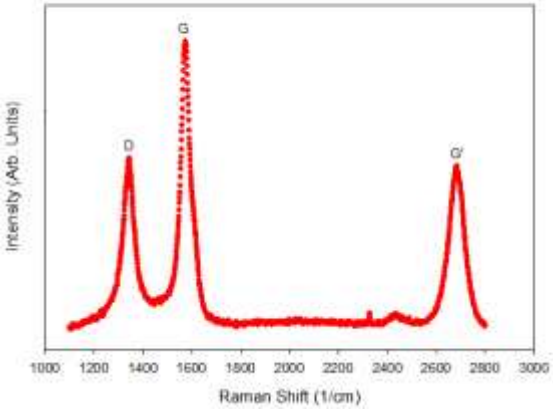

MKNano Spot 3

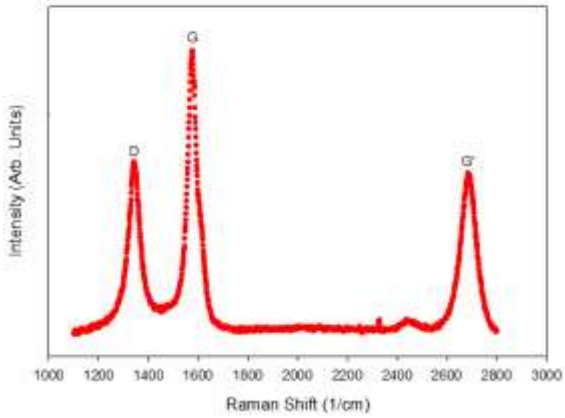

MKNano Spot 4

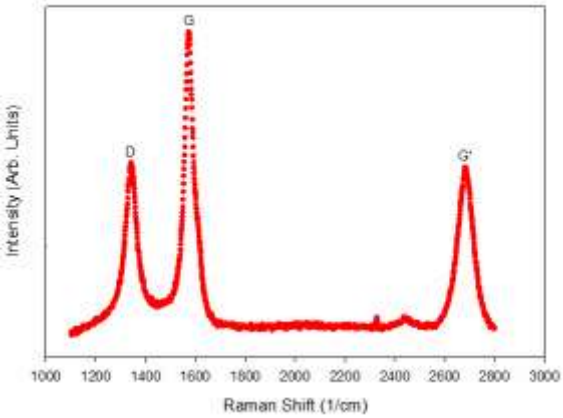

MKNano Spot 5

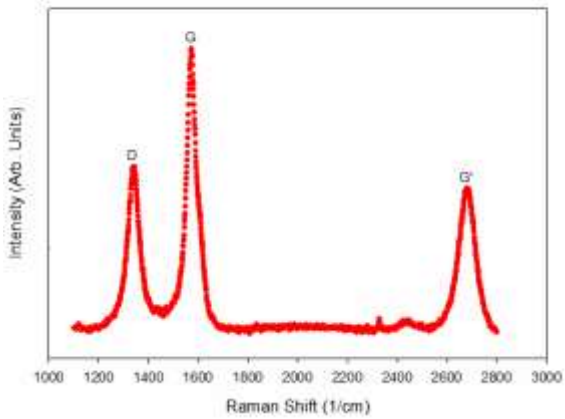

A.10 Sigma Aldrich

Sigma Aldrich Spot 1

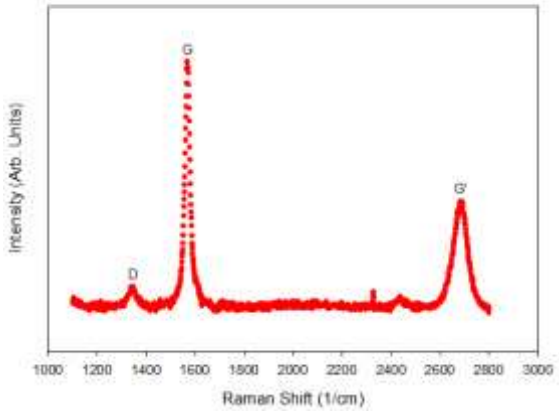

Sigma Aldrich Spot 2

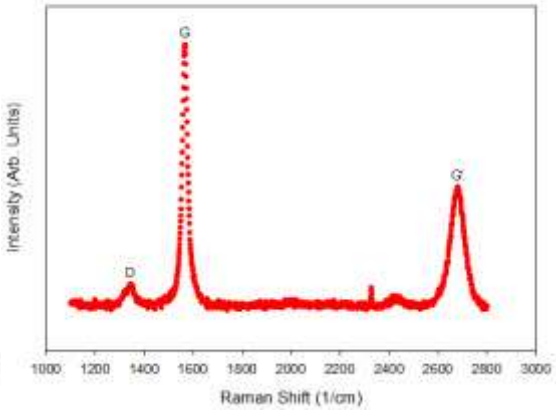

Sigma Aldrich Spot 3

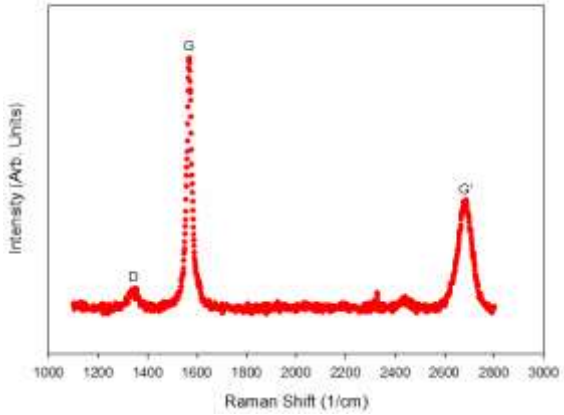

Sigma Aldrich Spot 4

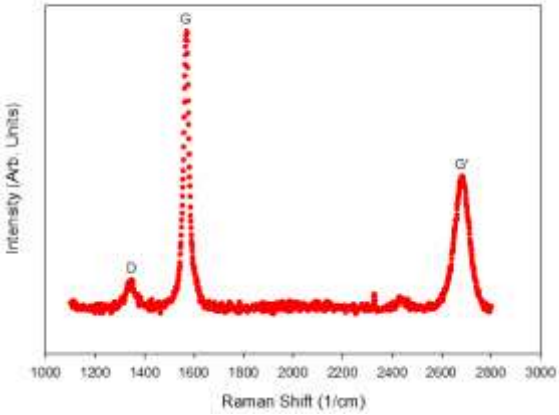

Sigma Aldrich Spot 5

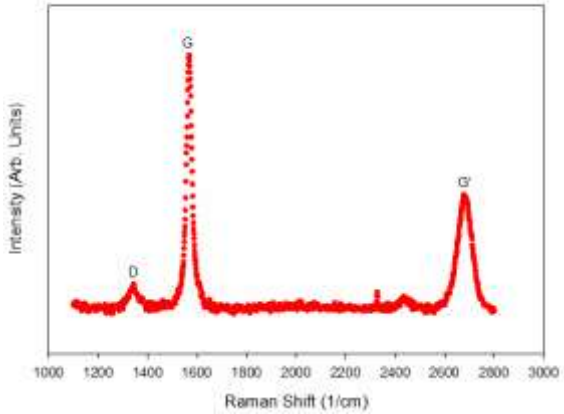

A.11 Nanoshel

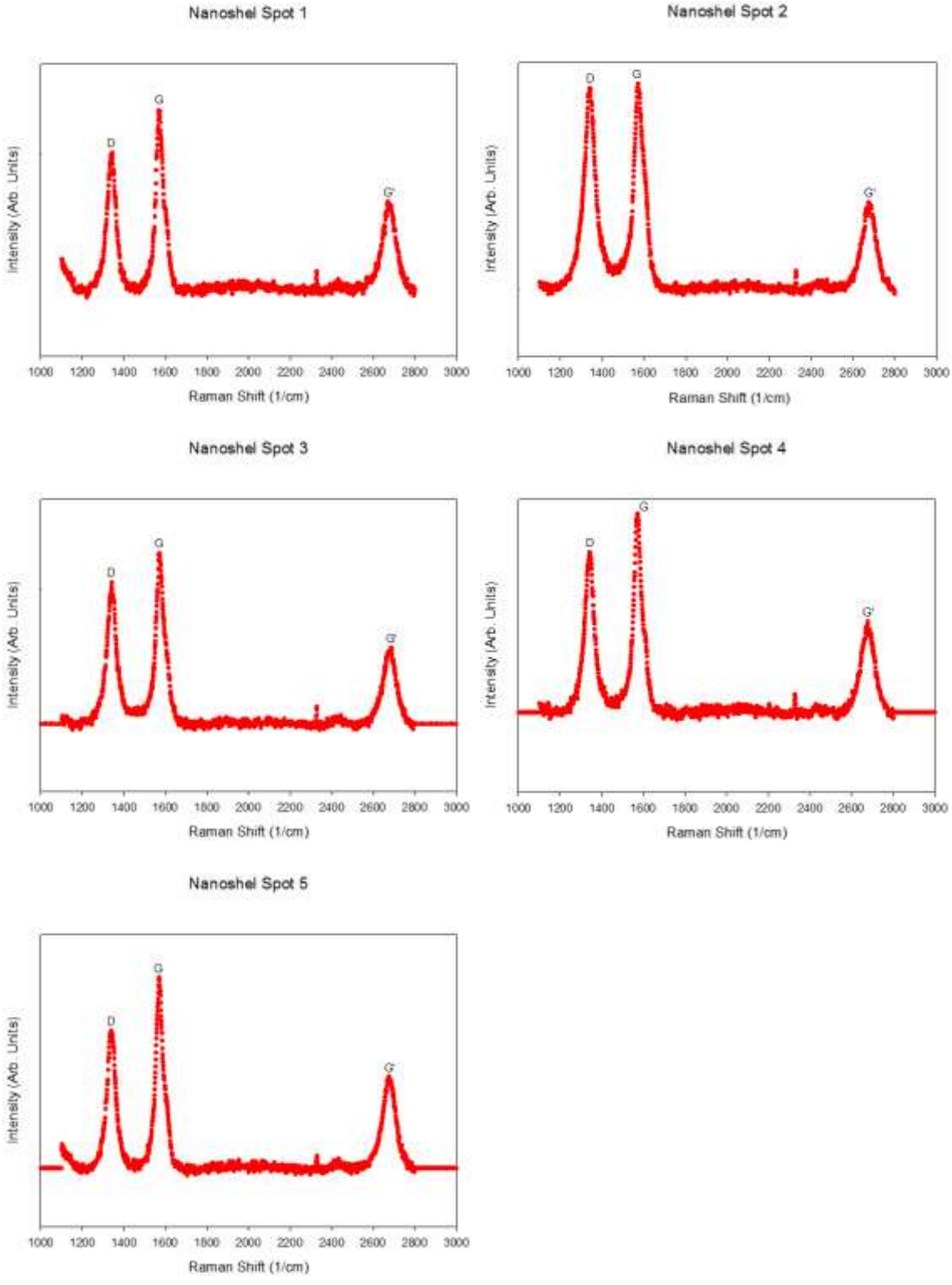

A.12 Nanoshel Arc-Discharged

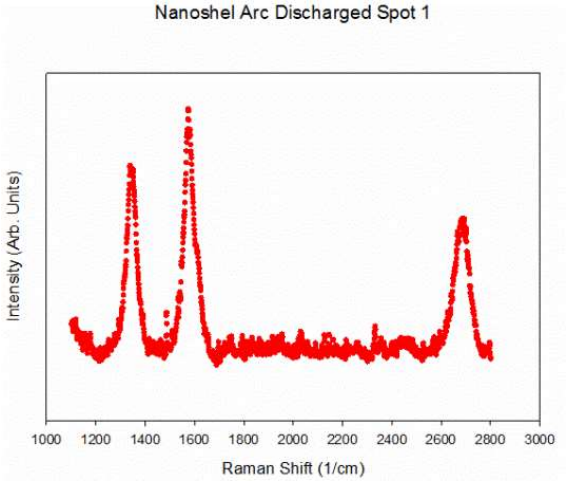

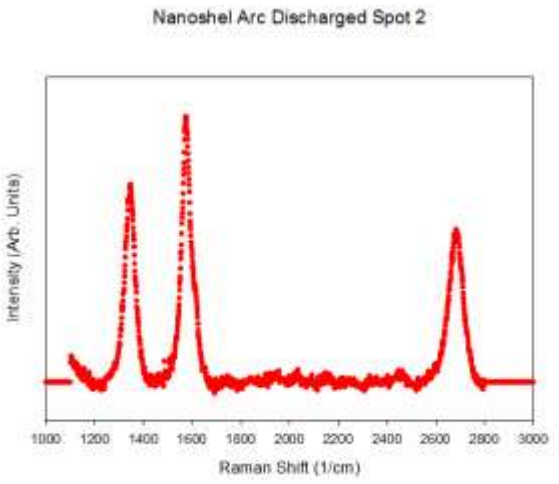

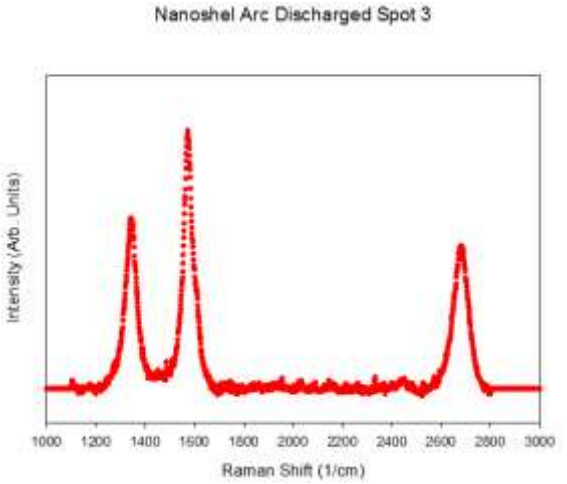

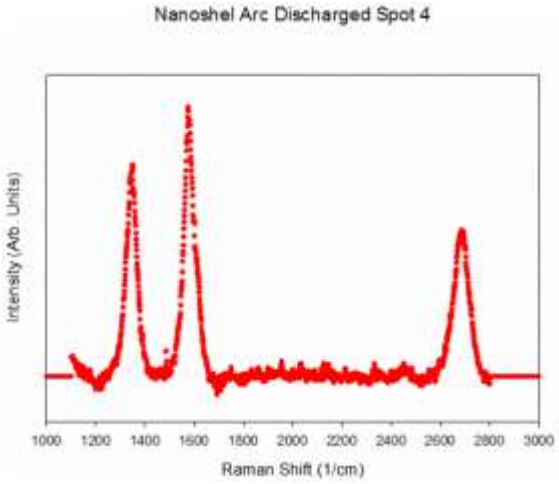

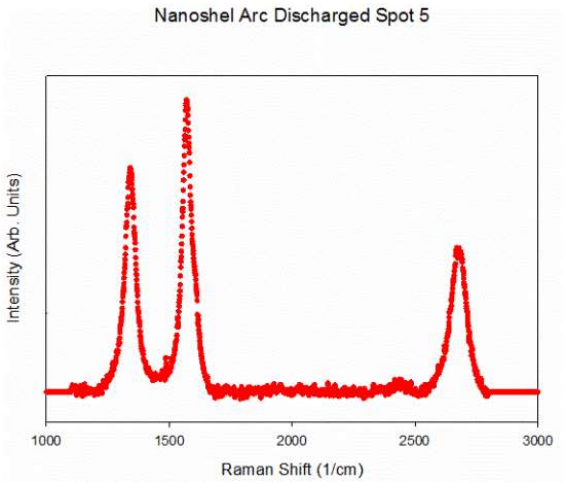

A.13 Ted Pella

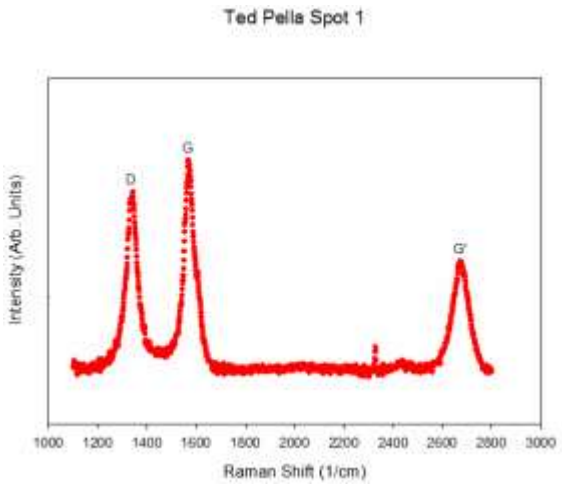

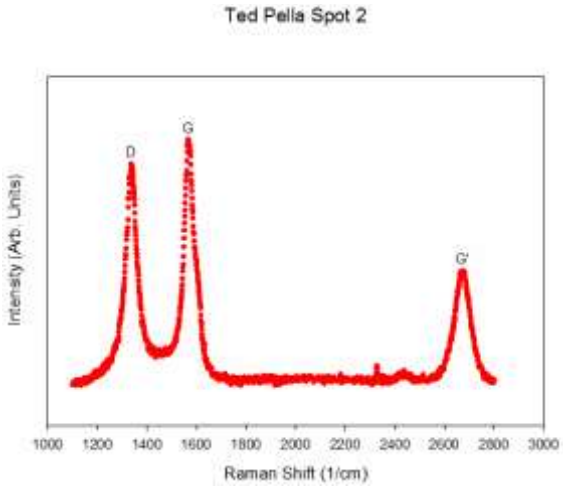

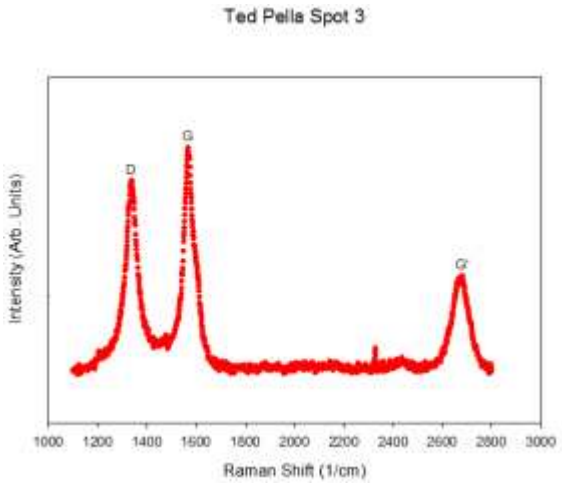

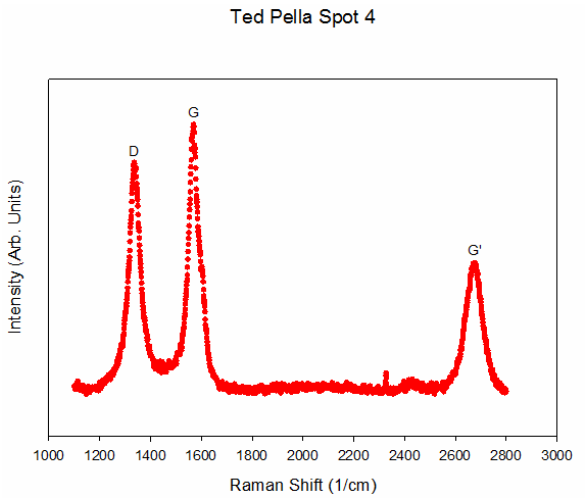

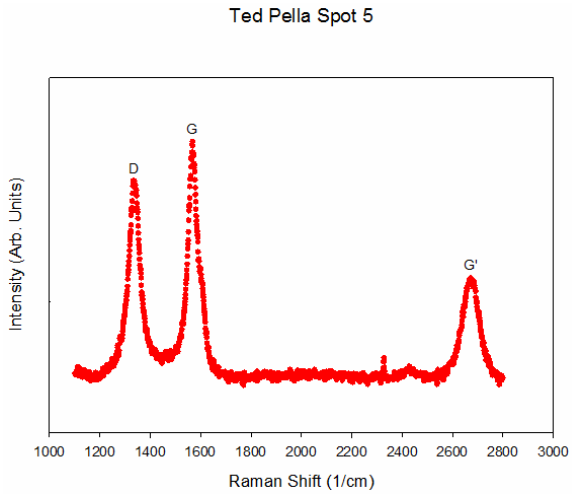

A.14 General Nano

General Nano Spot 1

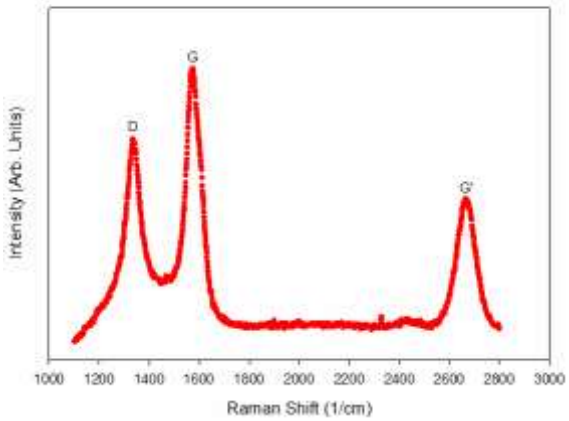

General Nano Spot 2

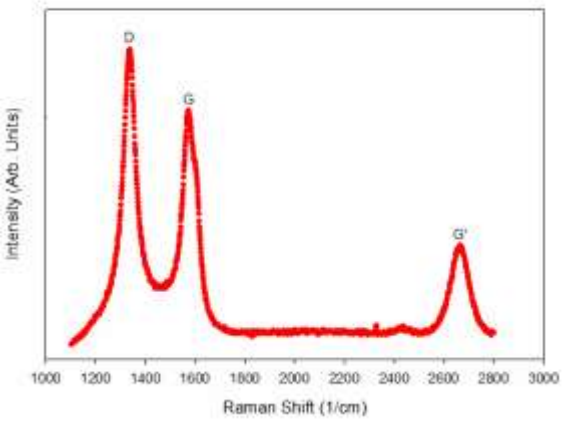

General Nano Spot 3

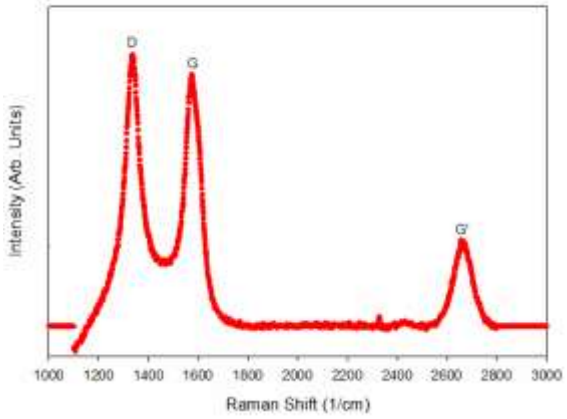

General Nano Spot 4

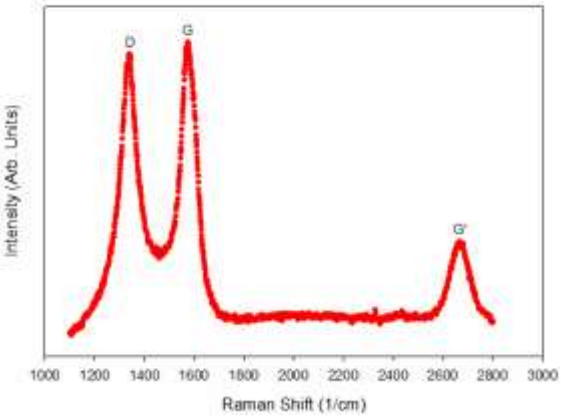

General Nano Spot 5

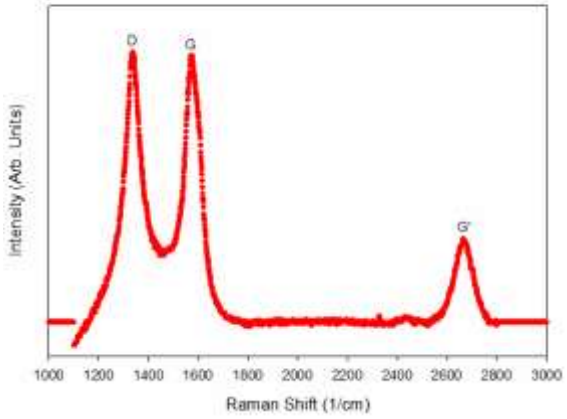

A.15 Pyrograf

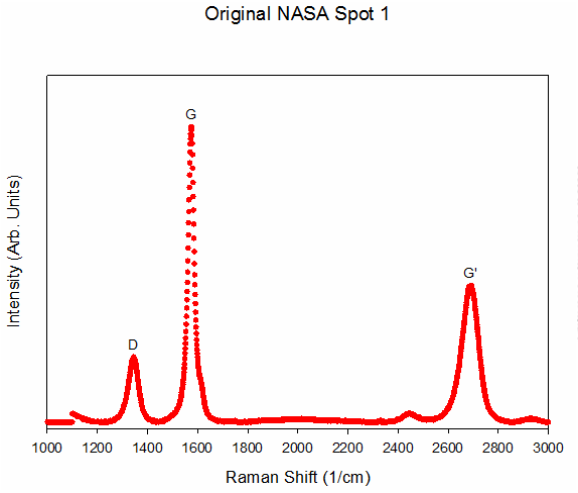

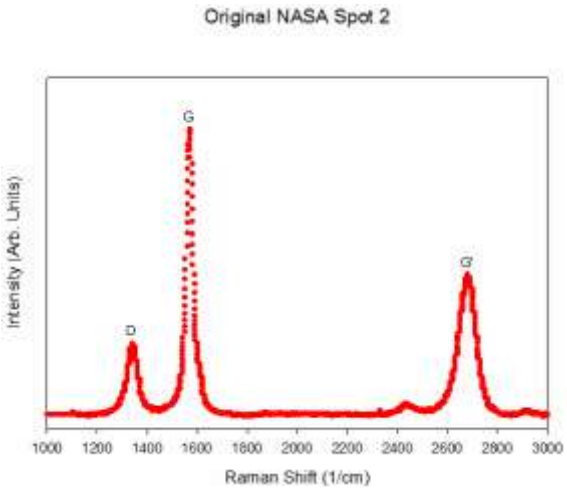

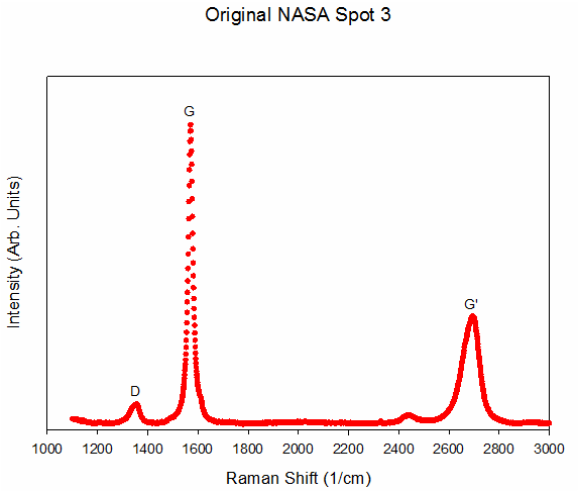

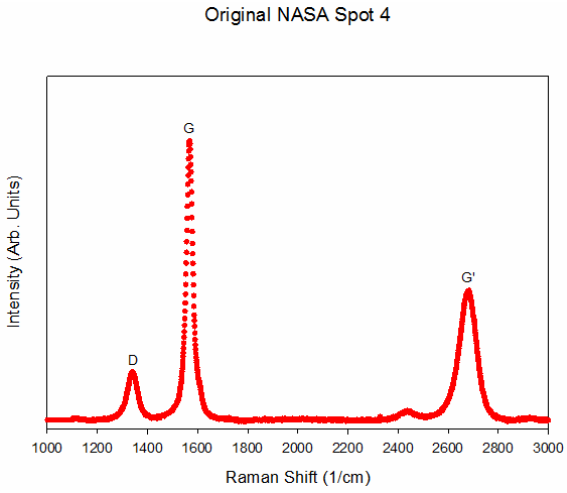

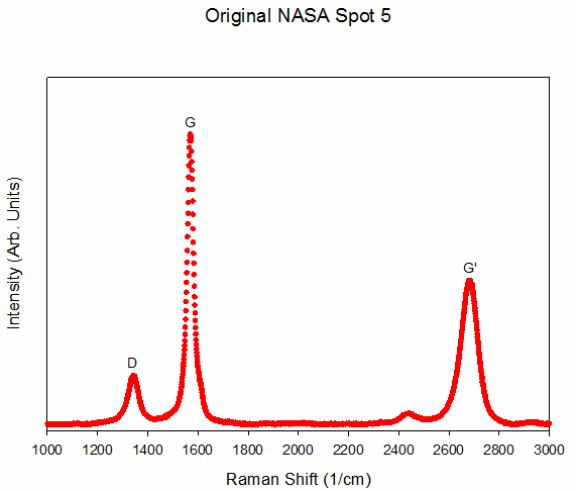

A.16 Case Western University

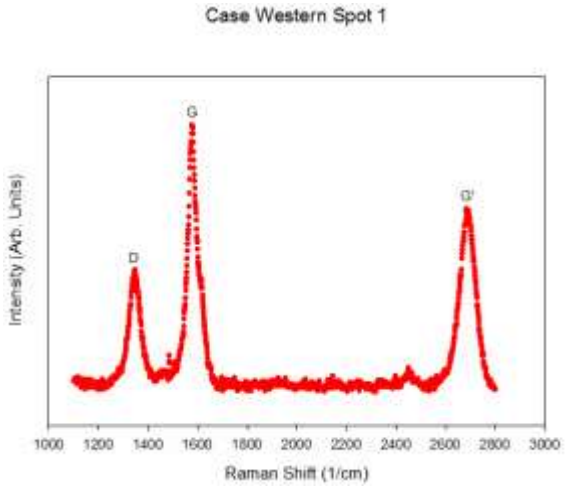

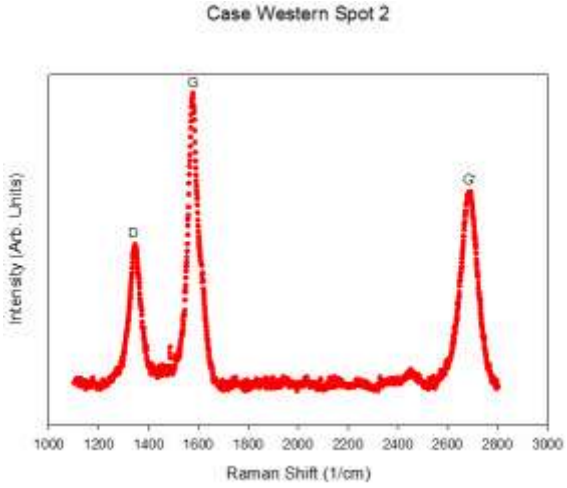

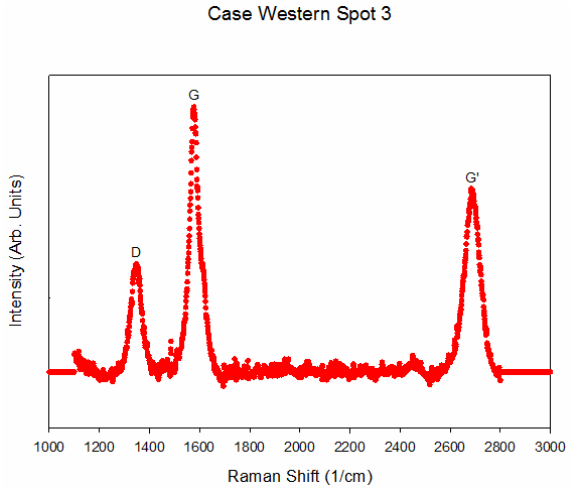

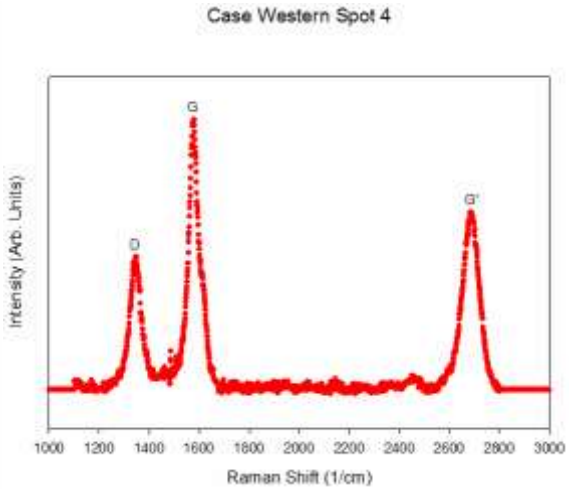

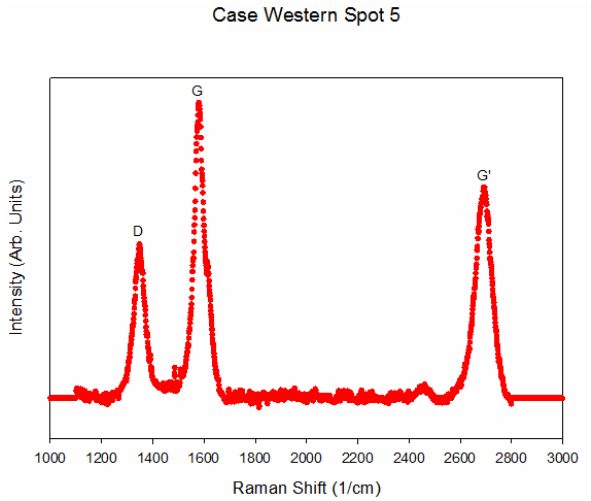

REFERENCES

Asheghi, M., Leung, Y. K., Wong, S. S., and Goodson, K. E., 1997, "Phonon-Boundary Scattering in Thin Silicon Layers," Appl. Phys. Lett. Vol. 71, pp. 1798 - 1800.

Berber, S., Y.-K. Kwon, et al. (2000). "Unusually High Thermal Conductivity of Carbon Nanotubes." Physical Review Letters **84**(20): 4613-4616.

Brown, E., L. Hao, et al. (2005). "Ballistic thermal and electrical conductance measurements on individual multiwall carbon nanotubes." Applied Physics Letters **87**(2): 023107.

Cahill, D. G., W. K. Ford, et al. (2003). "Nanoscale thermal transport." Journal of Applied Physics **93**(2): 793.

Cheaptubes.com. Graphetized MWCNT produt list. 22 April 2013.

Chen, Z., W. Jang, et al. (2009). "Thermal contact resistance between graphene and silicon dioxide." Applied Physics Letters **95**(16): 161910.

Chiu, H. Y., V. Deshpande, et al. (2005). "Ballistic Phonon Thermal Transport in Multiwalled Carbon Nanotubes." Physical Review Letters **95**(22).

Choi, T.-Y., D. Poulikakos, et al. (2006). "Measurement of the Thermal Conductivity of Individual Carbon Nanotubes by the Four-Point Three-omega Method." Nano Letters **6**(8): 1589-1593.

Coleman, H. W. and W. G. Steele (2009). Experimentation, Validation, and Uncertainty Analysis for Engineers. Hoboken, New Jersey, John Wiley & Sons, Inc.

Dames, C., S. Chen et al. (2007). "A hot-wire probe for thermal measurements of nanowires and nanotubes inside a transmission electron microsocope." Review of Scientific Insturents **78**: 104903.

Fujii, M., X. Zhang, et al. (2005). "Measuring the Thermal Conductivity of a Single Carbon Nanotube." Physical Review Letters **95**(6).

Hull, R. (1999). Properties of crystalline silicon, The Institution of Engineering and Technology.

Iijima, S. (1991). "Helical microtubes of graphitic carbon." Nature **354**, 56-58.

Li, Q., C. Liu, et al. (2009). "Measuring the thermal conductivity of individual carbon nanotubes by the Raman shift method." Nanotechnology **20**(14): 145702.

Li, W., Zhang, H., et al. (1997). "Raman characterization of aligned carbon nanotubes produced by thermal decomposition of hydrocarbon vapor." Applied Physics Letters **70**: 2684.

Lu, X., Shen W. Z., and Chu J.H. (2002). "Size effect on the thermal conductivity of nanowires." Journal of Applied Physics **91**(3): 1542

Keesom, W. H. and A. P. Keesom (1936). "On the heat conductivity of liquid helium." Physica **3**(5): 359-360.

Kim, P. (2002). "Mesoscopic thermal transport and energy dissipation in carbon nanotubes." Physica B: Condensed Matter **323**(1-4): 67-70.

Kim, P., L. Shi, et al. (2001). "Thermal Transport Measurements of Individual Multiwalled Nanotubes." Physical Review Letters **87**(21).

Kittel, Charles. *Introduction to Solid State Physics.* 8th edition. Hoboken, John Wiley & Sons, 2005. Print.

Kurti, N., B. V. Rollin, et al. (1936). "Preliminary experiments on temperature equilibria at very low temperatures." Physica **3**(1-4): 266-274.

Mingo, N. and D. A. Broido (2005). "Carbon Nanotube Ballistic Thermal Conductance and Its Limits." Physical Review Letters **95**: 096105.

Mirmira, S. R. and L. S. Fletcher (1998). "Review of the Thermal Conductivity of Thin Films." Journal of Thermophysics and Heat Transfer **12**(2): 121-131.

Ou M., Yang T., et al. (2008). "Electrical and thermal transport in single nickel nanowire." Applied Physics Letters **92**: 063101.

Patel, H.E., Beena George et al. (2003). "Thermal conductivities of naked and monolayer protected metal nanoparticle based nanofluids: Manifestation of anomalous enhancement and chemical effects." Applied Physics Letters **83**: 2931.

Pop, E., D. Mann, et al. (2006). "Thermal Conductance of an Individual Single-Wall Carbon Nanotube above Room Temperature." Nano Letters **6**(1): 96-100.

Prasher, Ravi. (2008). "Thermal boundary resistance and thermal conductivity of multiwalled carbon nanotubes." Physical Review B **77**: 075424.

Swartz, E.T., and Pohl R.O. (1987). "Thermal resistance at interfaces." Applied Physics Letters **51**: 2200.

Shi, L. "Data Processing Uncertainty Analysis Version 4." unpublished.

Shi, L., D. Li, et al. (2003). "Measuring Thermal and Thermoelectric Properties of One-Dimensional Nanostructures Using a Microfabricated Device." Journal of Heat Transfer **125**(5): 881.

StanfordResearchSystems (2007). manual of SR850 DSP Lock-In Amplifier. Sunnyvale, Stanford Research Systems.

Stewart D., and Norris P., (2000). "Size Effects on the Thermal Conductivity of Thin Metallic Wires: Microscale Implications." Microscale Thermophysical Engineering **4**: 89-100.

Swartz, E. T. and R. O. Pohl (1989). "Thermal boundary resistance." Reviews of Modern Physics **61**(3): 605-668.

Tighe, T. S., J. M. Worlock, et al. (1997). "Direct thermal conductance measurements on suspended monocrystalline nanostructures." Applied Physics Letters **70**(20): 2687-2689.

Yang, J., Waltermire S., Chen Y., Zinn A., Xu T., and Li D. (2010). "Contact thermal resistance between individual multiwall carbon nanotubes." Applied Physics Letters **96:** 023109.

Yang, J., Yang Y., Waltermire S., Gutu T., Zinn A., Xu T., Chen Y., and Li D. (2011) "Measurement of the Intrinsic Thermal Conductivity of a Multiwalled Carbon Nanotube and Its Contact Thermal Resistance with the Substrate." Small, **7**(16), 2334-2340.

Yu, C., L. Shi, et al. (2005). "Thermal Conductance and Thermopower of an Individual Single-Wall Carbon Nanotube." Nano Letters **5**(9): 1842-1846.

Zhang Q., Cao B., and Zhang X., (2006). "Influence of grain boundary scattering on the electrical and thermal conductivities of polycrystalline gold nanofilms." Physical Review B **74**: 134109.